Inverse Problems and Imaging
Volume 8, No. 3, 2014, 645–683
doi:10.3934/ipi.2014.8.645

RESOLUTION ENHANCEMENT FROM SCATTERING IN PASSIVE SENSOR IMAGING WITH CROSS CORRELATIONS

Josselin Garnier
Laboratoire de Probabilités et Modèles Aléatoires
& Laboratoire Jacques-Louis Lions
Université Paris Diderot
75205 Paris Cedex 13, France

George Papanicolaou
Mathematics Department, Stanford University
Stanford, CA 94305, USA

(Communicated by Margaret Cheney)

Abstract. It was shown in [Garnier et al., SIAM J. Imaging Sciences 2 (2009), 396] that it is possible to image reflectors by backpropagating cross correlations of signals generated by ambient noise sources and recorded at passive sensor arrays. The resolution of the image depends on the directional diversity of the noise signals relative to the locations of the sensor array and the reflector. When directional diversity is limited it is possible to enhance it by exploiting the scattering properties of the medium since scatterers will act as secondary noise sources. However, scattering increases the fluctuation level of the cross correlations and therefore tends to destabilize the image by reducing its signal-to-noise ratio. In this paper we study the trade-off in passive, correlation-based imaging between resolution enhancement and signal-to-noise ratio reduction that is due to scattering.

1. **Introduction.** It has been shown recently that the Green's function of the wave equation in an inhomogeneous medium can be estimated by cross correlating signals emitted by ambient noise sources and recorded by a passive sensor array [1, 9, 29, 30]. The cross correlation $C(\tau, \boldsymbol{x}_1, \boldsymbol{x}_2)$ of the signals recorded at two sensors $\boldsymbol{x}_1$ and $\boldsymbol{x}_2$:

$$C(\tau, \boldsymbol{x}_1, \boldsymbol{x}_2) = \frac{1}{T} \int_0^T u(t, \boldsymbol{x}_1) u(t+\tau, \boldsymbol{x}_2) \mathrm{d}t$$

is related to the Green's function between $\boldsymbol{x}_1$ and $\boldsymbol{x}_2$. In a homogeneous medium and when the source of the waves is a space-time stationary random field that is also delta-correlated in space and time, it has been shown [25, 21] that the τ-derivative of the cross correlation of the recorded signals is proportional to the symmetrized Green's function between the sensors (ie the difference of the causal and anticausal Green's functions):

$$\frac{\partial}{\partial \tau} C(\tau, \boldsymbol{x}_1, \boldsymbol{x}_2) \simeq -\left[G(\tau, \boldsymbol{x}_1, \boldsymbol{x}_2) - G(-\tau, \boldsymbol{x}_1, \boldsymbol{x}_2) \right], \tag{1}$$

2010 *Mathematics Subject Classification.* Primary: 35R30, 35R60; Secondary: 86A15, 78A46.
Key words and phrases. Passive sensor imaging, ambient noise sources, scattering media.
The authors thank the Institut des Hautes Études Scientifiques (IHÉS) for its hospitality while part of this work was done. The work of G. Papanicolaou was supported in part by AFOSR grant FA9550-11-1-0266. The work of J. Garnier was supported in part by ERC Advanced Grant Project MULTIMOD-267184.

 ©2014 American Institute of Mathematical Sciences

where G is the causal Green's function. In an inhomogeneous medium and when the sources completely surround the region of the sensors the approximate identity (1) is still valid and it can be shown using the Helmholtz-Kirchhoff theorem [29, 13]. This is true even with spatially localized noise source distributions provided the waves propagate within an ergodic cavity [1]. More generally, in an inhomogeneous medium the cross correlation as a function of the lag time τ can have a distinguishable peak at plus or minus the inter-sensor travel time $\mathcal{T}(\boldsymbol{x}_1, \boldsymbol{x}_2)$, provided the ambient noise sources are well distributed around the sensors and scattering by the inhomogeneities in the region between $\boldsymbol{x}_1$ and $\boldsymbol{x}_2$ is weak. The inter-sensor travel times obtained from peaks of cross correlations can then be used tomographically for background velocity estimation [2, 6, 17, 23, 31]. However, when the ambient noise sources have spatially limited support, the signals recorded by the sensors are generated by wave energy flux coming from the direction of the noise sources, which results in an azimuthal dependence of the quality of travel time estimation [27]. In general, travel time estimation by cross correlation of noise signals is possible when the line between the sensors is along the general direction of the energy flux and difficult or impossible when it is perpendicular to it. This can be explained and analyzed using the stationary phase method [4, 13, 16]. It is, however, possible to enhance the quality of travel time estimates by exploiting the increased directional diversity provided by the scattering of waves in a randomly inhomogeneous medium [13, 26]. We consider this briefly in Section 6.

Cross correlations of signals emitted by ambient noise sources and recorded by a passive sensor array can also be used for imaging of reflectors as was shown in [17, 13, 14]. The data that is used for imaging is the matrix of cross correlations $(C(\tau, \boldsymbol{x}_j, \boldsymbol{x}_l))_{j,l=1,\ldots,N}$ between pairs of sensors $(\boldsymbol{x}_j)_{j=1,\ldots,N}$. The objective is to image reflectors in the medium. In this paper we consider the two imaging functionals that use this data set and were introduced in [13, 14], corresponding to daylight and backlight illumination as described in the next paragraph. The form of these two functionals is motivated by the analysis in a homogeneous medium of the cross correlation matrix in the asymptotic regime in which the coherence time of the sources is small compared to typical travel times. These imaging functionals can also be applied in inhomogeneous media which is what is studied in this paper. We briefly review here the resolution results of [14] and analyze in detail the signal-to-noise ratio (SNR) of the imaging functionals. We only consider here images of single point reflectors and the SNR is defined as the mean of the image at the reflector position divided by the standard deviation of the image, also at the reflector position.

We consider relatively simple models for the reflector and the background medium that allow for a rather complete analysis that explains the main phenomena of interest when scattering is weak. In particular we show that resolution and SNR are not independent imaging attributes in a randomly scattering medium. In the analysis we use the Born approximation [5, 19, 11] for the reflectors and a single- and double-scattering approximations for the random medium. We also use extensively the stationary phase method [4]. We carry out numerical simulations to illustrate the results. This confirms that the theoretical predictions obtained in asymptotic regimes can be observed.

Homogeneous background medium. We summarize the main results in [13, 14] when the background medium is homogeneous. When there is only one reflector located at $\boldsymbol{z}_{\rm r}$, the cross correlation $C(\tau, \boldsymbol{x}_j, \boldsymbol{x}_l)$ between the two sensors at

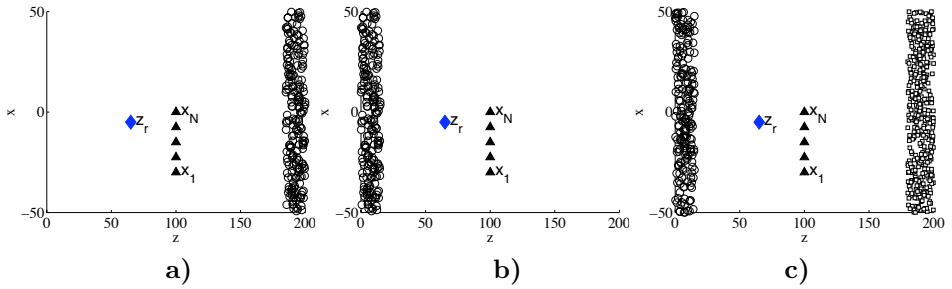

Figure 1. Passive sensor imaging using cross correlations of ambient noise signals. The circles indicate the location of the noise sources, the triangles that of the sensors, and the diamond that of the reflector. Figure (a) shows a daylight illumination configuration. Figure (b) shows a backlight illumination configuration. Figure (c) shows a primary backlight illumination configuration where the scatterers, indicated by squares, play the role of secondary sources providing a daylight illumination.

$\boldsymbol{x}_j$ and $\boldsymbol{x}_l$ can have additional peaks at lag times that are different from the inter-sensor travel times. Stationary phase analysis [13] shows that these additional peaks appear at lag times equal to either the sum or the difference between the travel times from the sensors to the reflector. This suggests that the reflector can be imaged by backpropagating or migrating the cross correlation matrix of the recorded signals because migration imaging exploits effectively these peaks. This form of passive sensor array imaging depends in an essential way on the illumination configuration, that is, the relative positions of the sensors, the noise sources and the reflector as follows:

- If the noise sources are spatially localized and the sensors are between the sources and the reflector, then additional peaks in the cross correlations occur at lag times equal to plus or minus the sum of travel times $\mathcal{T}(\boldsymbol{x}_l, \boldsymbol{z}_r) + \mathcal{T}(\boldsymbol{x}_j, \boldsymbol{z}_r)$. We call this the daylight configuration (see Figure 1a).
- If the noise sources are spatially localized and the reflector is between the sources and the sensors, then an additional peak in the cross correlations occurs at lag time equal to the difference of travel times $\mathcal{T}(\boldsymbol{x}_l, \boldsymbol{z}_r) - \mathcal{T}(\boldsymbol{x}_j, \boldsymbol{z}_r)$. We call this the backlight configuration (see Figure 1b).

The imaging functional that we use depends therefore on the illumination configuration. To form an image in a daylight illumination configuration, each element of the cross correlation matrix is evaluated at lag time equal to the sum of the travel times $\mathcal{T}(\boldsymbol{x}_l, \boldsymbol{z}^S) + \mathcal{T}(\boldsymbol{z}^S, \boldsymbol{x}_j)$ between the sensor $\boldsymbol{x}_l$ and a search point $\boldsymbol{z}^S$ in the image domain, and between the search point $\boldsymbol{z}^S$ and the sensor $\boldsymbol{x}_j$. The daylight imaging functional is the sum of the migrated matrix elements over all pairs of sensors, as discussed in Subsection 3.3. To form an image in a backlight illumination configuration, each element of the cross correlation matrix is evaluated at lag time equal to the difference of the travel times $\mathcal{T}(\boldsymbol{x}_l, \boldsymbol{z}^S) - \mathcal{T}(\boldsymbol{z}^S, \boldsymbol{x}_j)$ and the migrated matrix elements are summed over all pairs of sensors. The backlight imaging functional has poor range resolution because it exploits only differences of travel times, which are much less sensitive to the range than the sums of travel times [14].

Randomly scattering medium. The main result of this paper is a detailed analysis of how wave scattering affects both the resolution and the SNR of passive sensor imaging when using cross correlations of noise signals. We show in Section 4 that the scattering medium enhances the directional diversity of waves, which in turn can improve the resolution of the imaging functional. We show also that the random fluctuations in the cross correlations due to the scattering reduce the SNR of the imaging functional. These are the two competing phenomena that we analyze here in detail in a regime of weak scattering.

It is known that scattering by random inhomogeneities in the medium can enhance the directional diversity of waves leading to radiative transport and diffusion of wave energy [22]. In the context of time-reversal experiments it has been shown that time-reversal refocusing can be enhanced in a randomly scattering medium [11, 20]. This was also considered in the context of travel time estimation by cross correlation of noisy signals [13, 26].

We consider passive sensor imaging with cross correlations in configurations such as the one shown in Figure 1c. In such configurations the noise sources (on the left in Figure 1c) provide directly only backlight illumination, which leads to images with bad resolution but high SNR, while the scatterers (on the right in Figure 1c) provide a secondary daylight illumination, which leads to images with good resolution but low SNR. We address in this paper the quantification of this trade-off between resolution enhancement versus SNR reduction by scattering. We compute both the heights and widths of the peaks of the cross correlation at special lag times associated with the peaks influencing the migration functionals. We also calculate the standard deviations of the fluctuations of the cross correlations due to scattered waves. The main results of the SNR analysis at the peak in the cross correlations generated by the secondary illumination from the scatterers are summarized in Subsection 4.7. We also discuss a simple way to benefit from the advantages of both illuminations (ie, the direct and secondary illuminations) in a single imaging functional in Subsection 6.2.

A particular result of the analysis is that when the scattering region is far enough from the sensor array then migrating directly the cross correlations works well, as the theory of Section 4 predicts and as shown in Figure 7c. However, in unfavorable scattering situations the peaks generated by the secondary illumination are weak compared to the random fluctuations of the cross correlations. An example is given in Section 6 where the scattering region is too close to the sensor array. As a consequence migration of the cross correlation matrix gives the blurred and speckled image shown in Figure 12b. This is a typical example where the potential resolution enhancement is not achieved because of low SNR. In order to enhance the SNR we time window the cross correlations, select the tails (or coda) and cross correlate them. By migrating this special fourth-order cross correlation matrix it is possible to get a much better image than by migrating directly the cross correlation matrix. This is what we show in Section 6 but we do not have a complete mathematical analysis of the SNR for this kind of use of fourth-order cross correlations. Some analysis of fourth-order cross correlations in travel time estimation is given in [13].

When scattering is very strong then imaging with cross correlations cannot be done with migration or related coherent imaging methods. Fluctuations in the cross correlations from wave scattering are then large and the resulting low SNR becomes a limiting factor in image formation [15].

The paper is organized as follows. In Section 2 we introduce the framework for the analysis of cross correlations of noise signals. In Section 3 imaging by cross correlation of noise signals is reviewed briefly for a homogeneous background. Section 4 contains the main results of the paper, which address cross correlation based, passive array imaging in a weakly scattering medium. In Section 5 we consider the case in which scattering is not generated by random inhomogeneities but by a deterministic reflecting interface in the medium. In Section 6 we show how the use of iterated (fourth-order) cross correlations and appropriate imaging functionals can improve the resolution and SNR of passive sensor imaging in a scattering medium.

2. The cross correlation of ambient noise signals.

2.1. The wave equation with noise sources.

We consider the solution u of the wave equation in a three-dimensional inhomogeneous medium with propagation speed $c(\boldsymbol{x})$:

$$\frac{1}{c^2(\boldsymbol{x})}\frac{\partial^2 u}{\partial t^2} - \Delta_{\boldsymbol{x}} u = n(t,\boldsymbol{x}). \tag{2}$$

The propagation speed $c(\boldsymbol{x})$ may have a background part and localized changes (to be imaged). The background part can be homogeneous (this case is addressed in Section 3) or randomly heterogeneous (this case is addressed in Section 4).

The term $n(t,\boldsymbol{x})$ models a random field of noise sources. It is a zero-mean stationary (in time) random process with autocorrelation function

$$\langle n(t_1,\boldsymbol{y}_1)n(t_2,\boldsymbol{y}_2)\rangle = F(t_2-t_1)K(\boldsymbol{y}_1)\delta(\boldsymbol{y}_1-\boldsymbol{y}_2). \tag{3}$$

Here $\langle\cdot\rangle$ stands for statistical average with respect to the distribution of the noise sources. For simplicity we assume that the process n has Gaussian statistics.

The time distribution of the noise sources is characterized by the correlation function $F(t_2-t_1)$, which is a function of t_2-t_1 only by time stationarity. The function F is normalized so that $F(0)=1$. The Fourier transform $\hat{F}(\omega)$ of the time correlation function $F(t)$ is a nonnegative, even, real-valued function proportional to the power spectral density of the sources:

$$\hat{F}(\omega) = \int F(t)e^{i\omega t}\mathrm{d}t. \tag{4}$$

The width of $\omega \to \hat{F}(\omega)$ is the bandwidth. It is inversely proportional to the width of $t \to F(t)$, which is the decoherence time.

The spatial distribution of the noise sources is characterized by the autocovariance function $\delta(\boldsymbol{y}_1-\boldsymbol{y}_2)K(\boldsymbol{y}_1)$. The process n is delta-correlated in space and the nonnegative function K characterizes the spatial support of the sources, assumed compact.

2.2. Statistical stability of the cross correlation function.

The stationary solution of the wave equation has the integral representation

$$u(t,\boldsymbol{x}) = \iint n(t-s,\boldsymbol{y})G(s,\boldsymbol{x},\boldsymbol{y})\mathrm{d}s\mathrm{d}\boldsymbol{y}, \tag{5}$$

where $G(t,\boldsymbol{x},\boldsymbol{y})$ is the time-dependent outgoing Green's function. It is the fundamental solution of the wave equation

$$\frac{1}{c^2(\boldsymbol{x})}\frac{\partial^2 G}{\partial t^2} - \Delta_{\boldsymbol{x}} G = \delta(t)\delta(\boldsymbol{x}-\boldsymbol{y}), \tag{6}$$

starting from $G(0,\boldsymbol{x},\boldsymbol{y}) = \partial_t G(0,\boldsymbol{x},\boldsymbol{y}) = 0$ (and continued on the negative time axis by $G(t,\boldsymbol{x},\boldsymbol{y}) = 0$, $\forall t \le 0$).

The empirical cross correlation of the signals recorded at $\boldsymbol{x}_1$ and $\boldsymbol{x}_2$ for an integration time T is

$$C_T(\tau,\boldsymbol{x}_1,\boldsymbol{x}_2) = \frac{1}{T}\int_0^T u(t,\boldsymbol{x}_1)u(t+\tau,\boldsymbol{x}_2)\mathrm{d}t. \tag{7}$$

It is a statistically stable quantity, in the sense that for a large integration time T, the empirical cross correlation C_T is independent of the realization of the noise sources. This is stated in the following proposition proved in [13].

Proposition 1. *1. The expectation of the empirical cross correlation C_T (with respect to the distribution of the sources) is independent of T:*

$$\langle C_T(\tau,\boldsymbol{x}_1,\boldsymbol{x}_2)\rangle = C^{(1)}(\tau,\boldsymbol{x}_1,\boldsymbol{x}_2), \tag{8}$$

where the statistical cross correlation $C^{(1)}$ is given by

$$C^{(1)}(\tau,\boldsymbol{x}_1,\boldsymbol{x}_2) = \frac{1}{2\pi}\iint \mathrm{d}\boldsymbol{y}\mathrm{d}\omega \hat{F}(\omega)K(\boldsymbol{y})\overline{\hat{G}}(\omega,\boldsymbol{x}_1,\boldsymbol{y})\hat{G}(\omega,\boldsymbol{x}_2,\boldsymbol{y})e^{-i\omega\tau}, \tag{9}$$

and $\hat{G}(\omega,\boldsymbol{x},\boldsymbol{y})$ is the time-harmonic Green's function (i.e. the Fourier transform of $G(t,\boldsymbol{x},\boldsymbol{y})$).

2. The empirical cross correlation C_T is a self-averaging quantity:

$$C_T(\tau,\boldsymbol{x}_1,\boldsymbol{x}_2) \overset{T\to\infty}{\longrightarrow} C^{(1)}(\tau,\boldsymbol{x}_1,\boldsymbol{x}_2), \tag{10}$$

in probability with respect to the distribution of the sources.

2.3. **Small decoherence time hypothesis.** We assume from now on that the decoherence time of the noise sources is much smaller than the typical travel time that we want to estimate, that is, the travel time from the reflector(s) to the sensor array. If we denote by ε the (small) ratio of these two time scales, then we can write the time correlation function F_ε of the noise sources in the form

$$F_\varepsilon(t_2-t_1) = F\Big(\frac{t_2-t_1}{\varepsilon}\Big), \tag{11}$$

where t_1 and t_2 are scaled relative to typical travel times. The hypothesis $\varepsilon \ll 1$ is both natural and useful:

1) In surface wave tomography in geophysics, noise records are first bandpass-filtered and then cross correlated [23]. If the central frequency ω_0 of the filter, within the noise source bandwidth, is high enough so that the corresponding wavelength λ_0 is small compared to the distance d from the sensor array to the reflector, then we have $\varepsilon = \lambda_0/d \ll 1$. As we will see below, the range resolution of migration imaging by cross correlation is inversely proportional to the bandwidth, so the hypothesis $\varepsilon \ll 1$ turns out to be natural in order to get some resolution.

2) The Fourier transform $\hat{F}_\varepsilon$ of the time correlation function of the sources F_ε has the form $\hat{F}_\varepsilon(\omega) = \varepsilon\hat{F}(\varepsilon\omega)$, so that the statistical cross correlation (9) (after substituting $\hat{F}_\varepsilon(\omega)$ for $\hat{F}(\omega)$ and after the change of variables $\omega \to \omega/\varepsilon$) involves a product of Green's functions evaluated at high frequencies:

$$\begin{aligned} C^{(1)}(\tau,\boldsymbol{x}_1,\boldsymbol{x}_2) &= \frac{1}{2\pi}\iint \mathrm{d}\boldsymbol{y}\mathrm{d}\omega \hat{F}_\varepsilon(\omega)K(\boldsymbol{y})\overline{\hat{G}}(\omega,\boldsymbol{x}_1,\boldsymbol{y})\hat{G}(\omega,\boldsymbol{x}_2,\boldsymbol{y})e^{-i\omega\tau} \\ &= \frac{1}{2\pi}\iint \mathrm{d}\boldsymbol{y}\mathrm{d}\omega \hat{F}(\omega)K(\boldsymbol{y})\overline{\hat{G}}\Big(\frac{\omega}{\varepsilon},\boldsymbol{x}_1,\boldsymbol{y}\Big)\hat{G}\Big(\frac{\omega}{\varepsilon},\boldsymbol{x}_2,\boldsymbol{y}\Big)e^{-i\frac{\omega}{\varepsilon}\tau}. \end{aligned} \tag{12}$$

If the medium is smooth and if we can use a high-frequency approximation of the Green's function, then the stationary phase method [4] can be used in the regime $\varepsilon \ll 1$, as was done in [13]

3. **Passive sensor imaging with cross correlations in a homogeneous background medium.** In this section we revisit the results of [13, 14] and show that it is possible to image reflectors by cross correlations of signals generated by ambient noise sources and recorded by passive sensors.

We want to image reflectors in the medium from signals recorded by the array of sensors located at $(\boldsymbol{x}_j)_{j=1,\dots,N}$. In active array imaging the sensors can be used as emitters as well as receivers. The data set collected is the impulse response matrix $(P(t,\boldsymbol{x}_j,\boldsymbol{x}_l))_{j,l=1,\dots,N,t\in\mathbb{R}}$, where the (j,l)-entry of this matrix is the signal $(P(t,\boldsymbol{x}_j,\boldsymbol{x}_l))_{t\in\mathbb{R}}$ recorded by the jth sensor when the lth sensor emits a Dirac impulse. The usual migration techniques [3, 8] that backpropagate the impulse responses numerically in a fictitious medium produce images of the reflectors. However, in passive sensor imaging the sensors of the array do not have emission capacity and they can only act as receivers. The data collected in passive array imaging are the signals $(u(t,\boldsymbol{x}_j))_{t\in\mathbb{R}}$ generated by ambient noise sources and recorded by the jth sensor $j=1,\dots,N$. It turns out that the matrix of cross correlations of the recorded signals $(C(\tau,\boldsymbol{x}_j,\boldsymbol{x}_l))_{j,l=1,\dots,N,\tau\in\mathbb{R}}$ (with C defined as in (7)) behaves like the impulse response matrix of an active sensor array. It is therefore possible to image the reflectors by backpropagating the cross correlations.

3.1. **Differential cross correlations.** In order to image reflectors with cross correlations it is often necessary to have available data sets $\{C(\tau,\boldsymbol{x}_j,\boldsymbol{x}_l)\}_{j,l=1,\dots,N}$ and $\{C_0(\tau,\boldsymbol{x}_j,\boldsymbol{x}_l)\}_{j,l=1,\dots,N}$, with and without the reflectors, respectively, so that we can compute the differential cross correlations $\{C-C_0\}$ and migrate them. In general, the primary data set $\{C\}$ cannot be used directly for imaging because peaks in the cross correlations due to the reflectors may be very weak compared both to the peaks of the direct waves, at lag times equal to the inter-sensor travel times, as well as to the non-singular components due to the directionality of the energy flux [13]. This is so both in homogeneous and in scattering media. By singular component of a cross correlation we mean the leading contribution for ε small coming from the stationary phase approximation. By non-singular component we mean the remainder beyond the stationary phase approximation.

When the peaks in the cross correlations due to the reflectors to be imaged are well separated from peaks at inter-sensor travel times and from effects from noise energy flux directionality, we may be able to migrate directly the cross correlations of the primary data set $\{C(\tau,\boldsymbol{x}_j,\boldsymbol{x}_l)\}_{j,l=1,\dots,N}$. This issue is discussed in detail in Section 6 in [13].

3.2. **Stationary phase analysis.** In this section we review the analysis of the peaks of the cross correlations when the background medium is homogeneous with background speed c_0 and there is a point reflector at $\boldsymbol{z}_{\mathrm{r}}$ [14]. Since we assume that the reflector is weak and small, we can use the point interaction approximation for the Green's function, discussed in detail in Subsection 4.1:

$$\hat{G}_{0,\mathrm{r}}(\omega,\boldsymbol{x},\boldsymbol{y}) = \hat{G}_0(\omega,\boldsymbol{x},\boldsymbol{y}) + \frac{\omega^2}{c_0^2}\sigma_{\mathrm{r}} l_{\mathrm{r}}^3 \hat{G}_0(\omega,\boldsymbol{x},\boldsymbol{z}_{\mathrm{r}})\hat{G}_0(\omega,\boldsymbol{z}_{\mathrm{r}},\boldsymbol{y}), \tag{13}$$

σ_{r} is the reflectivity of the point reflector and l_{r}^3 is the effective scattering volume. Here $\hat{G}_0$ is the Green's function of the homogeneous background medium, that is,

in the absence of reflector,

$$\hat{G}_0(\omega,\boldsymbol{x},\boldsymbol{y}) = \frac{1}{4\pi|\boldsymbol{x}-\boldsymbol{y}|}e^{i\omega\mathcal{T}(\boldsymbol{x},\boldsymbol{y})}, \qquad \mathcal{T}(\boldsymbol{x},\boldsymbol{y}) = \frac{|\boldsymbol{x}-\boldsymbol{y}|}{c_0}, \tag{14}$$

where $\mathcal{T}(\boldsymbol{x},\boldsymbol{y})$ is the travel time between $\boldsymbol{x}$ and $\boldsymbol{y}$. The statistical differential cross correlation is given by

$$\Delta C_0^{(1)}(\tau,\boldsymbol{x}_1,\boldsymbol{x}_2) = C_{0,\mathrm{r}}^{(1)}(\tau,\boldsymbol{x}_1,\boldsymbol{x}_2) - C_0^{(1)}(\tau,\boldsymbol{x}_1,\boldsymbol{x}_2), \tag{15}$$

where $C_{0,\mathrm{r}}^{(1)}$ is the statistical cross correlation in the presence of the reflector, that is, equation (12) with the full Green's function (13). The cross correlation $C_0^{(1)}$ is obtained in the absence of the reflector, that is, equation (12) with the background Green's function (14). We collect the terms with the same power in σ_{r}. The terms of order $O(1)$ cancel and we retain only the terms of order $O(\sigma_{\mathrm{r}})$ consistent with the Born or lowest order scattering approximation:

$$\begin{aligned}\Delta C_0^{(1)}(\tau,\boldsymbol{x}_1,\boldsymbol{x}_2) = \frac{\sigma_{\mathrm{r}} l_{\mathrm{r}}^3}{2\pi c_0^2\varepsilon^2}\iint \mathrm{d}\boldsymbol{y}\mathrm{d}\omega K(\boldsymbol{y})\omega^2\hat{F}(\omega)\overline{\hat{G}_0}\Big(\frac{\omega}{\varepsilon},\boldsymbol{x}_1,\boldsymbol{y}\Big)\hat{G}_0\Big(\frac{\omega}{\varepsilon},\boldsymbol{x}_2,\boldsymbol{z}_{\mathrm{r}}\Big)\\ \times\hat{G}_0\Big(\frac{\omega}{\varepsilon},\boldsymbol{z}_{\mathrm{r}},\boldsymbol{y}\Big)e^{-i\frac{\omega\tau}{\varepsilon}}\\ +\frac{\sigma_{\mathrm{r}} l_{\mathrm{r}}^3}{2\pi c_0^2\varepsilon^2}\iint \mathrm{d}\boldsymbol{y}\mathrm{d}\omega K(\boldsymbol{y})\omega^2\hat{F}(\omega)\overline{\hat{G}_0}\Big(\frac{\omega}{\varepsilon},\boldsymbol{x}_1,\boldsymbol{z}_{\mathrm{r}}\Big)\overline{\hat{G}_0}\Big(\frac{\omega}{\varepsilon},\boldsymbol{z}_{\mathrm{r}},\boldsymbol{y}\Big)\\ \times\hat{G}_0\Big(\frac{\omega}{\varepsilon},\boldsymbol{x}_2,\boldsymbol{y}\Big)e^{-i\frac{\omega\tau}{\varepsilon}}.\end{aligned} \tag{16}$$

In the differential cross correlations the contributions of the direct waves are removed since they are common in the cross correlations in the presence and in the absence of the reflector. As a result the small singular components corresponding to the waves scattered by the reflector can be observed.

The next proposition 2 identifies the singular components of the differential cross correlations, which is useful to determine the appropriate imaging functional that should be used to migrate the cross correlations as we discuss in Subsection 3.3. This proposition is also the first step in the SNR analysis that we carry out in Section 4. It is proved in [14]. The proof uses stationary phase analysis for (16) in order to show that the singular contributions of the differential cross correlation correspond to (stationary) pairs of ray segments joining a source point $\boldsymbol{y}$ (ie a point in the support of K), the reflector $\boldsymbol{z}_{\mathrm{r}}$, and the sensors $\boldsymbol{x}_1$ and $\boldsymbol{x}_2$. The proposition shows that there are two main types of configurations of sources, sensors, and reflectors.

1) The noise sources are spatially localized and the sensors are between the sources and the reflectors (cases (a) and (b) in Figure 2). We call this the daylight illumination configuration. In this configuration the singular components of the differential cross correlation are concentrated at lag times equal to (plus or minus) the sum of travel times $\mathcal{T}(\boldsymbol{x}_2,\boldsymbol{z}_{\mathrm{r}}) + \mathcal{T}(\boldsymbol{x}_1,\boldsymbol{z}_{\mathrm{r}})$.

2) The noise sources are spatially localized and the reflectors are between the sources and the sensors (cases (c) and (d) in Figure 2). We call this the backlight illumination configuration. In this configuration the singular components of the differential cross correlation are concentrated at lag times equal to the difference of travel times $\mathcal{T}(\boldsymbol{x}_2,\boldsymbol{z}_{\mathrm{r}}) - \mathcal{T}(\boldsymbol{x}_1,\boldsymbol{z}_{\mathrm{r}})$.

Proposition 2. *In the backlight imaging configuration, in the regime $\varepsilon \to 0$, the differential cross correlation $\Delta C_0^{(1)}$ has a unique singular contribution at lag time*

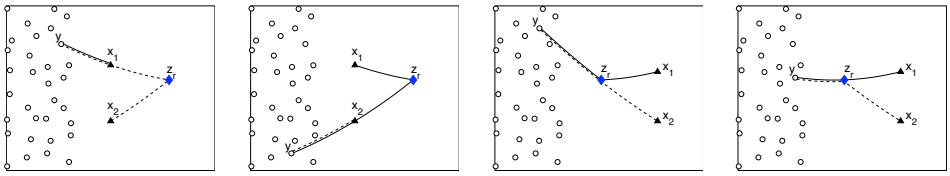

(a) **(b)** **(c)** **(d)**

Figure 2. Configurations of ray segments that contribute to the singular components of the differential cross correlation $\Delta C_0^{(1)}$ of noise signals between $\boldsymbol{x}_1$ and $\boldsymbol{x}_2$. The circles are noise sources, the triangles are sensors, and the diamond is the reflector. (a-b) are daylight configurations (the sensors are between the noise sources and the reflector), giving rise to a singular component at lag time equal to (plus or minus) the sum of travel times $\mathcal{T}(\boldsymbol{x}_1, \boldsymbol{z}_\mathrm{r}) + \mathcal{T}(\boldsymbol{x}_2, \boldsymbol{z}_\mathrm{r})$, (c-d) are backlight configurations (the reflector is between the noise sources and the sensors), giving rise to a singular component at lag time equal to the difference of travel times $\mathcal{T}(\boldsymbol{x}_2, \boldsymbol{z}_\mathrm{r}) - \mathcal{T}(\boldsymbol{x}_1, \boldsymbol{z}_\mathrm{r})$,

equal to the difference of travel times $\mathcal{T}(\boldsymbol{x}_2, \boldsymbol{z}_\mathrm{r}) - \mathcal{T}(\boldsymbol{x}_1, \boldsymbol{z}_\mathrm{r})$ *and it has the form:*

(17)
$$\Delta C_0^{(1)}(\tau, \boldsymbol{x}_1, \boldsymbol{x}_2) = \frac{\sigma_\mathrm{r} l_\mathrm{r}^3}{32\pi^2 c_0} \frac{K_{\boldsymbol{z}_\mathrm{r}, \boldsymbol{x}_1} - K_{\boldsymbol{z}_\mathrm{r}, \boldsymbol{x}_2}}{|\boldsymbol{z}_\mathrm{r} - \boldsymbol{x}_1||\boldsymbol{z}_\mathrm{r} - \boldsymbol{x}_2|} \partial_\tau F_\varepsilon\big(\tau - [\mathcal{T}(\boldsymbol{x}_2, \boldsymbol{z}_\mathrm{r}) - \mathcal{T}(\boldsymbol{x}_1, \boldsymbol{z}_\mathrm{r})]\big),$$

where $K_{\boldsymbol{z}, \boldsymbol{x}}$ *is the energy released by the noise sources along the ray in their support joining* $\boldsymbol{x}$ *and* $\boldsymbol{z}$ *expressed by*

(18)
$$K_{\boldsymbol{z}, \boldsymbol{x}} = \int_0^\infty K\Big(\boldsymbol{z} + \frac{\boldsymbol{z} - \boldsymbol{x}}{|\boldsymbol{z} - \boldsymbol{x}|} l\Big) \mathrm{d}l.$$

In the daylight illumination configuration, the differential cross correlation $\Delta C_0^{(1)}$ *has two singular contributions at lag times equal to plus or minus the sum of travel times* $\mathcal{T}(\boldsymbol{x}_2, \boldsymbol{z}_\mathrm{r}) + \mathcal{T}(\boldsymbol{x}_1, \boldsymbol{z}_\mathrm{r})$. *The peak centered at plus the sum of travel times has the form:*

(19)
$$\Delta C_0^{(1)}(\tau, \boldsymbol{x}_1, \boldsymbol{x}_2) = \frac{\sigma_\mathrm{r} l_\mathrm{r}^3}{32\pi^2 c_0} \frac{K_{\boldsymbol{x}_1, \boldsymbol{z}_\mathrm{r}}}{|\boldsymbol{z}_\mathrm{r} - \boldsymbol{x}_1||\boldsymbol{z}_\mathrm{r} - \boldsymbol{x}_2|} \partial_\tau F_\varepsilon\big(\tau - [\mathcal{T}(\boldsymbol{x}_2, \boldsymbol{z}_\mathrm{r}) + \mathcal{T}(\boldsymbol{x}_1, \boldsymbol{z}_\mathrm{r})]\big).$$

The peak centered at minus the sum of travel times has the form:

(20)
$$\Delta C_0^{(1)}(\tau, \boldsymbol{x}_1, \boldsymbol{x}_2) = \frac{-\sigma_\mathrm{r} l_\mathrm{r}^3}{32\pi^2 c_0} \frac{K_{\boldsymbol{x}_2, \boldsymbol{z}_\mathrm{r}}}{|\boldsymbol{z}_\mathrm{r} - \boldsymbol{x}_1||\boldsymbol{z}_\mathrm{r} - \boldsymbol{x}_2|} \partial_\tau F_\varepsilon\big(\tau + [\mathcal{T}(\boldsymbol{x}_2, \boldsymbol{z}_\mathrm{r}) + \mathcal{T}(\boldsymbol{x}_1, \boldsymbol{z}_\mathrm{r})]\big).$$

Note that Eq. (18) shows that $K_{\boldsymbol{z}_\mathrm{r}, \boldsymbol{x}_j}$ is nonnegative and it is positive only when the ray going from $\boldsymbol{x}_j$ to $\boldsymbol{z}_\mathrm{r}$ extends into the source region, which is the backlight illumination configuration, while $K_{\boldsymbol{x}_j, \boldsymbol{z}_\mathrm{r}}$ is positive only when the ray going from $\boldsymbol{z}_\mathrm{r}$ to $\boldsymbol{x}_j$ extends into the source region, which is the daylight illumination configuration. Proposition 2 shows that 1) the heights of the peaks are inversely proportional to the square of the distance from the reflector to the sensor array, 2) they do not depend on the distance from the sources to the reflector or the sensor array, and

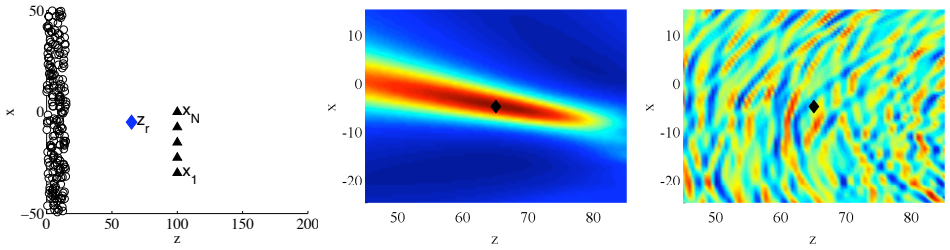

a) Configuration **b)** $\mathcal{I}^{\mathrm{B}}$ **c)** $\mathcal{I}^{\mathrm{D}}$

FIGURE 3. Passive sensor imaging using the differential cross correlation technique in a homogeneous medium. The backlight illumination configuration is shown in Figure a: the circles are the noise sources, the triangles are the sensors, and the diamond is the reflector. Figure b shows the image obtained with the backlight imaging functional (22). Figure c shows the image obtained with the daylight imaging functional (21).

3) they are proportional to the thickness of the source region, that is, the thickness of the support of K (see (18)). The second property was already noted in [14]. It is a consequence of two competing phenomena that cancel each other: on the one hand the geometric decay of the amplitude of the Green's function as a function of the distance from the sources to the reflector, and on the other hand the decay of the Hessian determinant of the phase at the stationary points, which by the stationary phase approximation produces a multiplicative factor in the evaluation of the integral (16).

3.3. **Migration imaging of cross correlations.** We consider first migration imaging with daylight illumination. The imaging functional at a search point $\boldsymbol{z}^S$ is the daylight imaging functional defined by [13]

$$\mathcal{I}^{\mathrm{D}}(\boldsymbol{z}^S) = \sum_{j,l=1}^{N} \Delta C\big(\mathcal{T}(\boldsymbol{z}^S,\boldsymbol{x}_l) + \mathcal{T}(\boldsymbol{z}^S,\boldsymbol{x}_j), \boldsymbol{x}_j, \boldsymbol{x}_l\big). \tag{21}$$

It is a consequence of Proposition 2 that the migration functional is obtained by summing the differential cross correlation at lag time equal to the sum of travel times $\mathcal{T}(\boldsymbol{z}^S,\boldsymbol{x}_l)+\mathcal{T}(\boldsymbol{z}^S,\boldsymbol{x}_j)$. Indeed it is shown there that the singular component of $\Delta C(\tau,\boldsymbol{x}_j,\boldsymbol{x}_l)$ is at $\tau = \pm[\mathcal{T}(\boldsymbol{z}_{\mathrm{r}},\boldsymbol{x}_l)+\mathcal{T}(\boldsymbol{z}_{\mathrm{r}},\boldsymbol{x}_j)]$. By summing ΔC over the sum of travel times $\mathcal{T}(\boldsymbol{z}^S,\boldsymbol{x}_l)+\mathcal{T}(\boldsymbol{z}^S,\boldsymbol{x}_j)$ the imaging functional $\mathcal{I}^{\mathrm{D}}(\boldsymbol{z}^S)$ presents a strong peak at the reflector location $\boldsymbol{z}^S = \boldsymbol{z}_{\mathrm{r}}$. The resolution analysis of the daylight imaging functional is carried out in [14]. The cross range resolution of the daylight imaging functional for a linear sensor array with aperture a is given by $\lambda_0 a/d(A,R)$. Here $d(A,R)$ is the distance between the sensor array and the reflector and λ_0 is the central wavelength. The range resolution for broadband noise sources is equal to c_0/B where c_0 is the background propagation speed and B is the bandwidth. The range resolution for narrowband noise sources is $\lambda_0 a^2/d(A,R)^2$. These resolution estimates are as in active array imaging in homogeneous media.

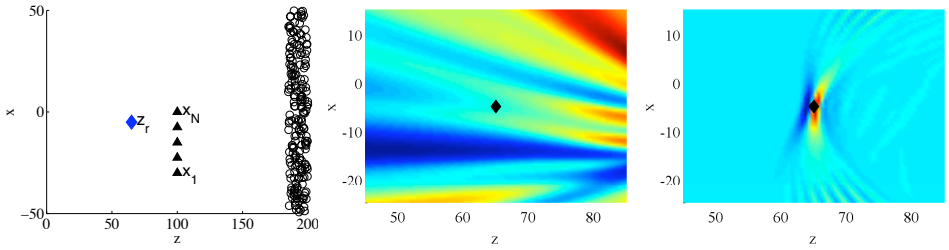

a) Configuration **b)** $\mathcal{I}^{\mathrm{B}}$ **c)** $\mathcal{I}^{\mathrm{D}}$

FIGURE 4. Passive sensor imaging using the differential cross correlation technique in a homogeneous medium. The daylight illumination configuration is shown in Figure a. Figure b shows the image obtained with the backlight imaging functional (22). Figure c shows the image obtained with the daylight imaging functional (21).

We consider next migration imaging with backlight illumination. The imaging functional at a search point $\boldsymbol{z}^S$ is the backlight imaging functional defined by [13]

$$\mathcal{I}^{\mathrm{B}}(\boldsymbol{z}^S) = \sum_{j,l=1}^{N} \Delta C(\mathcal{T}(\boldsymbol{z}^S, \boldsymbol{x}_l) - \mathcal{T}(\boldsymbol{z}^S, \boldsymbol{x}_j), \boldsymbol{x}_j, \boldsymbol{x}_l). \tag{22}$$

The sign of the travel time in the argument of the imaging functional is determined by Proposition 2. Indeed it is shown there that the singular component of $\Delta C(\tau, \boldsymbol{x}_j, \boldsymbol{x}_l)$ is at $\tau = \mathcal{T}(\boldsymbol{z}_{\mathrm{r}}, \boldsymbol{x}_l) - \mathcal{T}(\boldsymbol{z}_{\mathrm{r}}, \boldsymbol{x}_j)$. The resolution analysis of the backlight imaging functional is carried out in [14]. The cross range resolution is $\lambda_0 a/d(A,R)$ while the range resolution is $\lambda_0 a^2/d(A,R)^2$ whatever the bandwidth, which means that the range resolution is very poor compared to the daylight imaging functional.

3.4. **Numerical simulations.** In the numerical simulations presented here we evaluate the statistical cross correlations $C^{(1)}_{0,\mathrm{r}}$ and $C^{(1)}_0$ for different configurations of noise sources, reflector, and sensors. The statistical cross correlation is what is obtained with the empirical cross correlation C_T for an infinitely large integration time T. The statistical stability (i.e. the fact that the fluctuations of C_T with respect to its statistical average are small for finite T) can be characterized by the ratio of the standard deviation of the cross correlation over its mean. It has been studied in detail theoretically and numerically in [13], where it is shown that statistical stability is ensured provided the recording time window is sufficiently large.

We consider a three-dimensional homogeneous background medium with speed $c_0 = 1$. We compute the image in the plane (x, z) and use the homogeneous background Green's function (14). The random sources are a collection of 100 randomly located point sources in a layer of size 100×15 with power spectral density $\hat{F}(\omega) = \exp(-\omega^2)$. We consider a point reflector at position $(-5, 60)$ with reflectivity $\sigma_{\mathrm{r}} l_{\mathrm{r}}^3 = 0.01$ and 5 sensors located at $(-37.5 + 7.5j, 100)$, $j = 1, \ldots, 5$.

In Figure 3 we consider a backlight illumination configuration. We apply both the backlight imaging functional (22) and the daylight imaging functional (21). As predicted by the theory, the backlight imaging functional has good cross-range

resolution but very poor range resolution. The daylight imaging functional is not appropriate.

In Figure 4 we consider a daylight illumination configuration. We apply both the backlight imaging functional (22) and the daylight imaging functional (21). As predicted by the theory, the daylight imaging functional has good cross-range and range resolutions. The backlight imaging functional is not appropriate.

4. Passive sensor imaging in a randomly scattering medium.

In this section we consider imaging by cross correlations, as in the previous section, but in addition to the homogeneous background there are random inhomogeneities that cause scattering. In the first four subsections we formulate the multiple scattering problem and introduce the setup for the analysis of the differential cross correlations. In the following subsections we focus our attention on the backlight illumination configuration with scatterers behind the sensor array (see Figure 7a). This is an interesting configuration because the sources provide a backlight illumination and only the backlight imaging functional gives an image of the reflector in a homogeneous medium, as in Figure 3. In a scattering medium we anticipate that the scatterers have the advantage that they can enhance the directional diversity and provide a secondary daylight illumination, but they also have the drawback that they introduce fluctuations in the cross correlations. These are the phenomena that we want to analyze in detail. Subsections 4.5-4.7 give a quantitative analysis of the first two moments (mean and variance) of the differential cross correlation at appropriate lag times. Subsection 4.8 summarizes this quantitative analysis and applications to migration imaging are discussed in Subsection 4.9.

4.1. A model for the scattering medium.

In order to analyze the cross correlation technique in a scattering medium, we first introduce a model for the inhomogeneous medium. We assume that the speed of propagation of the medium has a homogeneous background speed value c_0 and small and weak fluctuations responsible for scattering:

$$\frac{1}{c_{\rm clu}^2(\boldsymbol{x})} = \frac{1}{c_0^2}\big[1+V(\boldsymbol{x})\big], \tag{23}$$

where $V(\boldsymbol{x})$ is a random process with mean zero and covariance function of the form

$$\mathbb{E}\big[V(\boldsymbol{x})V(\boldsymbol{x}')\big] = \sigma_{\rm s}^2 R(\boldsymbol{x},\boldsymbol{x}'). \tag{24}$$

Here $\mathbb{E}$ stands for the expectation with respect to the distribution of the randomly scattering medium, $\sigma_{\rm s}$ is the standard deviation of the fluctuations, and the function $\boldsymbol{x} \to R(\boldsymbol{x},\boldsymbol{x})$ characterizes the spatial support of the scatterers, assumed to be compact. The cluttered Green's function $\hat{G}_{\rm clu}$, that is to say, the Green's function of the medium with clutter in the absence of reflector, is the fundamental solution of

$$\Delta_{\boldsymbol{x}}\hat{G}_{\rm clu}\big(\omega,\boldsymbol{x},\boldsymbol{y}\big) + \frac{\omega^2}{c_{\rm clu}^2(\boldsymbol{x})}\hat{G}_{\rm clu}\big(\omega,\boldsymbol{x},\boldsymbol{y}\big) = -\delta(\boldsymbol{x}-\boldsymbol{y}), \tag{25}$$

with $c_{\rm clu}(\boldsymbol{x})$ given by (23) (along with a radiation condition).

We now assume that a reflector is embedded at $\boldsymbol{z}_{\rm r}$ in the cluttered medium. We model the reflector by a local variation $V_{\rm r}(\boldsymbol{x})$ of the speed of propagation:

$$\frac{1}{c^2(\boldsymbol{x})} = \frac{1}{c_0^2}\big[1+V(\boldsymbol{x})+V_{\rm r}(\boldsymbol{x})\big], \qquad V_{\rm r}(\boldsymbol{x}) = \sigma_{\rm r}\mathbf{1}_{\Omega_{\rm r}}(\boldsymbol{x}-\boldsymbol{z}_{\rm r}).$$

Here $\Omega_{\rm r}$ is a compactly supported domain with volume $l_{\rm r}^3$. The full Green's function $\hat{G}_{\rm clu,r}$, that is to say, the Green's function of the medium with clutter in the presence of the reflector at $\boldsymbol{z}_{\rm r}$, is solution of

$$\Delta_{\boldsymbol{x}}\hat{G}_{\rm clu,r}(\omega,\boldsymbol{x},\boldsymbol{y})+\frac{\omega^2}{c^2(\boldsymbol{x})}\hat{G}_{\rm clu,r}(\omega,\boldsymbol{x},\boldsymbol{y})=-\delta(\boldsymbol{x}-\boldsymbol{y}).$$

It can be written as the sum

$$\hat{G}_{\rm clu,r}(\omega,\boldsymbol{x},\boldsymbol{y})=\hat{G}_{\rm clu}(\omega,\boldsymbol{x},\boldsymbol{y})+\hat{G}_{\rm cor}(\omega,\boldsymbol{x},\boldsymbol{y}), \tag{26}$$

where the clutter Green's function $\hat{G}_{\rm clu}$ is solution of (25). The correction $\hat{G}_{\rm cor}$ is solution of the Helmholtz equation with propagation speed $c_{\rm clu}$ and the source term $-c_0^{-2}\omega^2 V_{\rm r}(\boldsymbol{x})\hat{G}_{\rm clu,r}(\omega,\boldsymbol{x},\boldsymbol{y})$:

$$\Delta_{\boldsymbol{x}}\hat{G}_{\rm cor}(\omega,\boldsymbol{x},\boldsymbol{y})+\frac{\omega^2}{c_{\rm clu}^2(\boldsymbol{x})}\hat{G}_{\rm cor}(\omega,\boldsymbol{x},\boldsymbol{y})=-\frac{\omega^2}{c_0^2}V_{\rm r}(\boldsymbol{x})\hat{G}_{\rm clu,r}(\omega,\boldsymbol{x},\boldsymbol{y}),$$

so that it can be represented as

$$\hat{G}_{\rm cor}(\omega,\boldsymbol{x},\boldsymbol{y})=\frac{\omega^2}{c_0^2}\int\hat{G}_{\rm clu}(\omega,\boldsymbol{x},\boldsymbol{z})V_{\rm r}(\boldsymbol{z})\hat{G}_{\rm clu,r}(\omega,\boldsymbol{z},\boldsymbol{y})\mathrm{d}\boldsymbol{z} \tag{27}$$

$$=\frac{\omega^2}{c_0^2}\int\hat{G}_{\rm clu}(\omega,\boldsymbol{x},\boldsymbol{z})V_{\rm r}(\boldsymbol{z})\big[\hat{G}_{\rm clu}(\omega,\boldsymbol{z},\boldsymbol{y})+\hat{G}_{\rm cor}(\omega,\boldsymbol{z},\boldsymbol{y})\big]\mathrm{d}\boldsymbol{z}. \tag{28}$$

This expression is exact and it is called the Lippmann-Schwinger equation [18]. The Born approximation (or single-scattering approximation) consists in substituting $\hat{G}_{\rm clu}$ for $\hat{G}_{\rm clu,r}$ on the right side of (27) (or equivalently neglecting $\hat{G}_{\rm cor}$ on the right side of (28)), which gives [5, section 13.1.2]:

$$\hat{G}_{\rm cor}(\omega,\boldsymbol{x},\boldsymbol{y})\simeq\frac{\omega^2}{c_0^2}\int\hat{G}_{\rm clu}(\omega,\boldsymbol{x},\boldsymbol{z})V_{\rm r}(\boldsymbol{z})\hat{G}_{\rm clu}(\omega,\boldsymbol{z},\boldsymbol{y})\mathrm{d}\boldsymbol{z}.$$

This approximation is formally valid if the correction $\hat{G}_{\rm cor}$ is small compared to $\hat{G}_{\rm clu}$, i.e., in the regime in which $\sigma_{\rm r}\ll 1$, with an error that is formally of order $O(\sigma_{\rm r}^2)$. We also assume that the diameter $l_{\rm r}$ of the scattering region $\Omega_{\rm r}$ is small compared to the typical wavelength. We can then model the reflector by a point reflector (the point interaction approximation)

$$V_{\rm r}(\boldsymbol{x})=\sigma_{\rm r}\mathbf{1}_{\Omega_{\rm r}}(\boldsymbol{x}-\boldsymbol{z}_{\rm r})\approx\sigma_{\rm r}l_{\rm r}^3\delta(\boldsymbol{x}-\boldsymbol{z}_{\rm r}),$$

and we can write the correction in the form

$$\hat{G}_{\rm cor}(\omega,\boldsymbol{x},\boldsymbol{y})=\frac{\omega^2}{c_0^2}\sigma_{\rm r}l_{\rm r}^3\hat{G}_{\rm clu}(\omega,\boldsymbol{x},\boldsymbol{z}_{\rm r})\hat{G}_{\rm clu}(\omega,\boldsymbol{z}_{\rm r},\boldsymbol{y}),$$

and with these approximations the full Green's function is

$$\hat{G}_{\rm clu,r}(\omega,\boldsymbol{x},\boldsymbol{y})=\hat{G}_{\rm clu}(\omega,\boldsymbol{x},\boldsymbol{y})+\frac{\omega^2}{c_0^2}\sigma_{\rm r}l_{\rm r}^3\hat{G}_{\rm clu}(\omega,\boldsymbol{x},\boldsymbol{z}_{\rm r})\hat{G}_{\rm clu}(\omega,\boldsymbol{z}_{\rm r},\boldsymbol{y}). \tag{29}$$

A mathematically rigorous analysis of these approximations, in random media, is not available to our knowledge. Interesting multiple scattering results are analyzed at a physical level in [24]. Detailed analysis of multiple scattering in randomly layered media, including layered interfaces, is carried out in [11]. But even in randomly layered media a detailed mathematical analysis of scattering by a small isotropic reflector has not been carried out, to our knowledge.

4.2. **The differential cross correlation.** We consider the statistical differential cross correlation, that is the difference between the statistical cross correlations in the presence and in the absence of reflector. It is given by

$$\Delta C^{(1)}(\tau,\boldsymbol{x}_1,\boldsymbol{x}_2) = C^{(1)}_{\rm clu,r}(\tau,\boldsymbol{x}_1,\boldsymbol{x}_2) - C^{(1)}_{\rm clu}(\tau,\boldsymbol{x}_1,\boldsymbol{x}_2), \tag{30}$$

$$C^{(1)}_{\rm clu,r}(\tau,\boldsymbol{x}_1,\boldsymbol{x}_2) = \frac{1}{2\pi}\iint {\rm d}\boldsymbol{y}{\rm d}\omega K(\boldsymbol{y})\hat{F}(\omega)\overline{\hat{G}_{\rm clu,r}}\Big(\frac{\omega}{\varepsilon},\boldsymbol{x}_1,\boldsymbol{y}\Big) \times\hat{G}_{\rm clu,r}\Big(\frac{\omega}{\varepsilon},\boldsymbol{x}_2,\boldsymbol{y}\Big)e^{-i\frac{\omega\tau}{\varepsilon}}, \tag{31}$$

$$C^{(1)}_{\rm clu}(\tau,\boldsymbol{x}_1,\boldsymbol{x}_2) = \frac{1}{2\pi}\iint {\rm d}\boldsymbol{y}{\rm d}\omega K(\boldsymbol{y})\hat{F}(\omega)\overline{\hat{G}_{\rm clu}}\Big(\frac{\omega}{\varepsilon},\boldsymbol{x}_1,\boldsymbol{y}\Big) \times\hat{G}_{\rm clu}\Big(\frac{\omega}{\varepsilon},\boldsymbol{x}_2,\boldsymbol{y}\Big)e^{-i\frac{\omega\tau}{\varepsilon}}, \tag{32}$$

where $\hat{G}_{\rm clu}$ is the clutter Green's function (36) in the absence of the reflector and $\hat{G}_{\rm clu,r}$ is the full Green's function (29) in the presence of the reflector. We substitute the approximation (29) into (30-31). Consistent with the Born approximation, we neglect the terms of order $O(\sigma_{\rm r}^2)$ in $\Delta C^{(1)}(\tau,\boldsymbol{x}_1,\boldsymbol{x}_2)$ and we find

$$\begin{aligned}\Delta C^{(1)}(\tau,\boldsymbol{x}_1,\boldsymbol{x}_2) = {}& \frac{\sigma_{\rm r} l_{\rm r}^3}{2\pi c_0^2\varepsilon^2}\iint {\rm d}\boldsymbol{y}{\rm d}\omega K(\boldsymbol{y})\omega^2\hat{F}(\omega)\overline{\hat{G}_{\rm clu}}\Big(\frac{\omega}{\varepsilon},\boldsymbol{x}_1,\boldsymbol{y}\Big)\hat{G}_{\rm clu}\Big(\frac{\omega}{\varepsilon},\boldsymbol{x}_2,\boldsymbol{z}_{\rm r}\Big) \\ &\times\hat{G}_{\rm clu}\Big(\frac{\omega}{\varepsilon},\boldsymbol{z}_{\rm r},\boldsymbol{y}\Big)e^{-i\frac{\omega\tau}{\varepsilon}} \\ &+\frac{\sigma_{\rm r} l_{\rm r}^3}{2\pi c_0^2\varepsilon^2}\iint {\rm d}\boldsymbol{y}{\rm d}\omega K(\boldsymbol{y})\omega^2\hat{F}(\omega)\overline{\hat{G}_{\rm clu}}\Big(\frac{\omega}{\varepsilon},\boldsymbol{x}_1,\boldsymbol{z}_{\rm r}\Big)\overline{\hat{G}_{\rm clu}}\Big(\frac{\omega}{\varepsilon},\boldsymbol{z}_{\rm r},\boldsymbol{y}\Big) \\ &\times\hat{G}_{\rm clu}\Big(\frac{\omega}{\varepsilon},\boldsymbol{x}_2,\boldsymbol{y}\Big)e^{-i\frac{\omega\tau}{\varepsilon}}.\end{aligned} \tag{33}$$

When the medium is homogeneous we recover the expression (16). When the medium is cluttered the expression (33) involves the clutter Green's function $\hat{G}_{\rm clu}$ solution of (25) that can have a complicated structure. We simplify the expression of the clutter Green's function in the next subsection in order to get a model that is mathematically tractable, and complex enough to explain the main phenomena we want to study, in terms of resolution enhancement and SNR reduction.

4.3. **Expansion of the clutter Green's function.** The Lippmann-Schwinger integral equation for the clutter Green's function $\hat{G}_{\rm clu}$ defined by (25) is

$$\hat{G}_{\rm clu}(\omega,\boldsymbol{x},\boldsymbol{y}) = \hat{G}_0(\omega,\boldsymbol{x},\boldsymbol{y}) + \frac{\omega^2}{c_0^2}\int \hat{G}_0(\omega,\boldsymbol{x},\boldsymbol{z})V(\boldsymbol{z})\hat{G}_{\rm clu}(\omega,\boldsymbol{z},\boldsymbol{y}){\rm d}\boldsymbol{z}, \tag{34}$$

where $\hat{G}_0$ is the Green's function (14) of the homogeneous background medium and $V(\boldsymbol{x})$ is the random process modeling the background fluctuations as described by (23). Iterating once this integral equation we have

$$\begin{aligned}\hat{G}_{\rm clu}(\omega,\boldsymbol{x},\boldsymbol{y}) = {}& \hat{G}_0(\omega,\boldsymbol{x},\boldsymbol{y}) + \frac{\omega^2}{c_0^2}\int \hat{G}_0(\omega,\boldsymbol{x},\boldsymbol{z})V(\boldsymbol{z})\hat{G}_0(\omega,\boldsymbol{z},\boldsymbol{y}){\rm d}\boldsymbol{z} \\ &+\frac{\omega^4}{c_0^4}\iint \hat{G}_0\big(\omega,\boldsymbol{x},\boldsymbol{z}\big)V(\boldsymbol{z})\hat{G}_0\big(\omega,\boldsymbol{z},\boldsymbol{z}'\big)V(\boldsymbol{z}')\hat{G}_{\rm clu}\big(\omega,\boldsymbol{z}',\boldsymbol{y}\big){\rm d}\boldsymbol{z}{\rm d}\boldsymbol{z}'.\end{aligned} \tag{35}$$

We will use the second order Born or multiple scattering approximation for the clutter Green's function solution of (35) by replacing $\hat{G}_{\rm clu}$ by $\hat{G}_0$ on the right side.

This approximation takes into account single and double scattering events for the interaction of the waves with the cluttered medium:

$$\hat{G}_{\rm clu}(\omega,\boldsymbol{x},\boldsymbol{y}) = \hat{G}_0(\omega,\boldsymbol{x},\boldsymbol{y}) + \hat{G}_1(\omega,\boldsymbol{x},\boldsymbol{y}) + \hat{G}_2(\omega,\boldsymbol{x},\boldsymbol{y}), \tag{36}$$

where $\hat{G}_1$ and $\hat{G}_2$ are given by

$$\hat{G}_1(\omega,\boldsymbol{x},\boldsymbol{y}) = \frac{\omega^2}{c_0^2}\int \hat{G}_0(\omega,\boldsymbol{x},\boldsymbol{z})V(\boldsymbol{z})\hat{G}_0(\omega,\boldsymbol{z},\boldsymbol{y})\mathrm{d}\boldsymbol{z}, \tag{37}$$

$$\hat{G}_2(\omega,\boldsymbol{x},\boldsymbol{y}) = \frac{\omega^4}{c_0^4}\iint \hat{G}_0(\omega,\boldsymbol{x},\boldsymbol{z})V(\boldsymbol{z})\hat{G}_0(\omega,\boldsymbol{z},\boldsymbol{z}')V(\boldsymbol{z}')\hat{G}_0(\omega,\boldsymbol{z}',\boldsymbol{y})\mathrm{d}\boldsymbol{z}\mathrm{d}\boldsymbol{z}', \tag{38}$$

and the error is formally of order $O(\sigma_s^3)$ where σ_s is the standard deviation of $V(\boldsymbol{x})$.

We take into account single and double scattering events because when scattering from the reflector described in the previous section is included, we collect and study all terms of order $O(\sigma_{\rm r})$, $O(\sigma_{\rm r}\sigma_{\rm s})$, and $O(\sigma_{\rm r}\sigma_{\rm s}^2)$ in the differential cross correlation in the approximate form (33), while we neglect all terms of order $O(\sigma_{\rm r}\sigma_{\rm s}^3)$ and $O(\sigma_{\rm r}^2)$. This means that we consider a regime in which $\sigma_{\rm r} \ll \sigma_{\rm s} \ll 1$. In words, scattering due to the random medium is weak, and the scattering due to the reflector is even weaker. That is why we have first expanded the differential cross correlation with respect to $\sigma_{\rm r}$, and then with respect to $\sigma_{\rm s}$. The reason we keep the term $\hat{G}_2$ in (36), which is of order $O(\sigma_s^2)$, is that in calculating moments of the differential cross correlation the lowest correction due to the random medium is of order $O(\sigma_s^2)$ and so consistency requires keeping all terms of this order.

In calculating means and variances of differential cross correlations, we make one more approximation. We assume that fluctuation covariance $R(\boldsymbol{x},\boldsymbol{x}')$ goes to zero rapidly when $\boldsymbol{x} \neq \boldsymbol{x}'$, which we express by writing

$$R(\boldsymbol{x},\boldsymbol{x}') = l_{\rm s}^3\rho(\boldsymbol{x})\delta(\boldsymbol{x}-\boldsymbol{x}'), \tag{39}$$

where $l_{\rm s}$ is a characteristic correlation length and $\rho(\boldsymbol{x})$ characterizes the spatial support of the scatterers, assumed to be compact.

A rigorous mathematical analysis for the above approximations is lacking at present. We know that in randomly layered media finite-order multiple scattering approximations are not correct, no matter how weak may be the random fluctuations in the medium [11]. This is because of wave localization. In three dimensions, multiple scattering in a random medium is analyzed mathematically using diagrammatic expansions [10] but the results needed here are not in the literature, to our knowledge. Formal multiple scattering expansions have been used extensively in random media [12, 28] for a long time.

4.4. **Expansion of the differential cross correlation.** By substituting the expansion (36) into (33) we can distinguish three contributions in the differential cross correlation:

$$\Delta C^{(1)}(\tau,\boldsymbol{x}_1,\boldsymbol{x}_2) = \Delta C_0^{(1)}(\tau,\boldsymbol{x}_1,\boldsymbol{x}_2) + \Delta C_1^{(1)}(\tau,\boldsymbol{x}_1,\boldsymbol{x}_2) + \Delta C_2^{(1)}(\tau,\boldsymbol{x}_1,\boldsymbol{x}_2), \tag{40}$$

where

- $\Delta C_0^{(1)}$ is the contribution of the direct waves (i.e. those which have not interacted with the random scatterers) which is given by (16),
- $\Delta C_1^{(1)}$ is the contributions of the waves that have been scattered once by the random scatterers, which is given by a sum of terms of the form (16) in which one of the factors $\hat{G}_0$ is replaced by $\hat{G}_1$,
- $\Delta C_2^{(1)}$ is the contributions of the waves that have been scattered twice by the

random scatterers, which is given by a sum of terms of the form (16) in which two of the factors $\hat{G}_0$ are replaced by $\hat{G}_1$ or one of the factors $\hat{G}_0$ is replaced by $\hat{G}_2$,
- we neglect higher-order terms as discussed in the previous section.

It turns out that in $\Delta C_2^{(1)}$ the second order scattering term $\hat{G}_2$ in (36) contributes neither to the mean to leading order, $\sigma_r\sigma_s^2$, nor to the standard deviation to leading order, $\sigma_r\sigma_s$, in the differential cross correlation. This is a result of the high-frequency (stationary phase) analysis when applied to the particular geometric configuration of the scattering region, the array and the reflector shown schematically in Figure 7a. It is not known in advance that such a result will hold, and it may not hold in other reflector-array-scattering region configurations. The calculations leading to this conclusion are presented in the second half of Appendix B. Thus, only the cross correlation terms that involve two (single-scattering) components $\hat{G}_1$ in (33) give a significant contribution to the mean and the variance of the overall cross correlation, while cross correlation terms that involve one (double-scattering) component $\hat{G}_2$ do not make any significant contribution.

4.5. **Statistical analysis of the differential cross correlation.** The contributions of the direct waves to the differential cross correlation are described in Proposition 2. In particular, the singular contribution (17) of the direct waves gives a peak to the backlight imaging functional (22) at the reflector location, but it does not give any contribution to the daylight imaging functional (21) at the reflector location.

We now analyze the contributions $\Delta C_1^{(1)}$ and $\Delta C_2^{(1)}$ of the scattered waves to the differential cross correlation in a backlight illumination configuration. Proposition 3 shows that scattering generates zero-mean random fluctuations in the cross correlations. This will reduce the SNR as we will discuss in the next subsections. Proposition 4 shows that scattering can increase the resolution of the image by enhancing directional diversity because it generates additional singular peaks in the cross correlations that are not present with only direct illumination, and they improve migration imaging.

The following proposition is proved in Appendix A. It describes the behavior of the first two moments of the cross correlation $\Delta C_1^{(1)}$. Here the mean and the variance are computed with respect to the distribution of the randomly scattering medium.

Proposition 3. *The contributions $\Delta C_1^{(1)}(\boldsymbol{x}_1,\boldsymbol{x}_2,\tau)$ have mean zero and variance whose leading-order terms are as follows.*

At lag time equal to the difference of travel times $\tau = \mathcal{T}(\boldsymbol{x}_2,\boldsymbol{z}_{\rm r}) - \mathcal{T}(\boldsymbol{x}_1,\boldsymbol{z}_{\rm r})$ the variance of the fluctuations is

$$\begin{aligned}
&\mathrm{Var}\big(\Delta C_1^{(1)}(\tau,\boldsymbol{x}_1,\boldsymbol{x}_2)\big)\\
&= \frac{\sigma_{\rm r}^2 l_{\rm r}^6 \sigma_{\rm s}^2 l_{\rm s}^3}{2^{14}\pi^6 c_0^5}\Big[\int \hat{F}_\varepsilon^2(\omega)\omega^6 \mathrm{d}\omega\Big]\Big[\frac{K^2_{\boldsymbol{x}_2,\boldsymbol{z}_{\rm r}}(\rho^{(i)}_{\boldsymbol{x}_1,\boldsymbol{z}_{\rm r}}+\rho^{(i)}_{\boldsymbol{x}_2,\boldsymbol{z}_{\rm r}}+2\rho^{(ii)}_{\boldsymbol{x}_2,\boldsymbol{z}_{\rm r}})}{|\boldsymbol{x}_1-\boldsymbol{z}_{\rm r}|^2|\boldsymbol{x}_2-\boldsymbol{z}_{\rm r}|^2}\\
&\quad+\frac{K^2_{\boldsymbol{x}_1,\boldsymbol{z}_{\rm r}}(\rho^{(i)}_{\boldsymbol{x}_1,\boldsymbol{z}_{\rm r}}+\rho^{(i)}_{\boldsymbol{x}_2,\boldsymbol{z}_{\rm r}}+2\rho^{(ii)}_{\boldsymbol{x}_1,\boldsymbol{z}_{\rm r}})}{|\boldsymbol{x}_1-\boldsymbol{z}_{\rm r}|^2|\boldsymbol{x}_2-\boldsymbol{z}_{\rm r}|^2}\Big],
\end{aligned} \tag{41}$$

where

$$\rho^{(i)}_{\boldsymbol{x}_j,\boldsymbol{z}_{\rm r}} = \int_0^1 \frac{\rho\big(\boldsymbol{x}_j+(\boldsymbol{z}_{\rm r}-\boldsymbol{x}_j)a\big)}{a(1-a)}\mathrm{d}a, \qquad \rho^{(ii)}_{\boldsymbol{x}_j,\boldsymbol{z}_{\rm r}} = \int_1^\infty \frac{\rho\big(\boldsymbol{x}_j+(\boldsymbol{z}_{\rm r}-\boldsymbol{x}_j)a\big)}{(a-1)a}\mathrm{d}a. \tag{42}$$

At lag time equal to the sum of travel times $\tau = \mathcal{T}(\boldsymbol{x}_2, \boldsymbol{z}_\mathrm{r}) + \mathcal{T}(\boldsymbol{x}_1, \boldsymbol{z}_\mathrm{r})$ *the variance of the fluctuations is*

$$\mathrm{Var}\big(\Delta C_1^{(1)}(\tau, \boldsymbol{x}_1, \boldsymbol{x}_2)\big) = \frac{\sigma_\mathrm{r}^2 l_\mathrm{r}^6 \sigma_\mathrm{s}^2 l_\mathrm{s}^3}{2^{15}\pi^7 c_0^5}\Big[\int \hat{F}_\varepsilon^2(\omega)\omega^6 \mathrm{d}\omega\Big] \frac{\rho^K_{\boldsymbol{x}_1,\boldsymbol{x}_2,\boldsymbol{z}_\mathrm{r}}}{|\boldsymbol{x}_1 - \boldsymbol{z}_\mathrm{r}|^2 |\boldsymbol{x}_2 - \boldsymbol{z}_\mathrm{r}|^2}, \tag{43}$$

where

$$\rho^K_{\boldsymbol{x}_1,\boldsymbol{x}_2,\boldsymbol{z}_\mathrm{r}} = 2\int_0^{2\pi} \mathrm{d}\psi \int_{-1}^1 \mathrm{d}v \frac{\big(K^2_{\boldsymbol{z}_\mathrm{r},\boldsymbol{x}_1} + K^2_{\boldsymbol{z}_\mathrm{r},\boldsymbol{z}(v,\psi)}\big)\rho(\boldsymbol{z}(v,\psi))}{u^2 - v^2}, \tag{44}$$

with

$$u = 1 + 2\frac{|\boldsymbol{x}_1 - \boldsymbol{z}_\mathrm{r}|}{|\boldsymbol{x}_2 - \boldsymbol{z}_\mathrm{r}|}, \qquad \boldsymbol{z}(v,\psi) = \frac{|\boldsymbol{x}_2 - \boldsymbol{z}_\mathrm{r}|}{2}\begin{pmatrix} vu \\ \sqrt{1-v^2}\sqrt{u^2-1}\cos\psi \\ \sqrt{1-v^2}\sqrt{u^2-1}\sin\psi \end{pmatrix}.$$

At lag time equal to minus the sum of travel times $\tau = -\mathcal{T}(\boldsymbol{x}_2, \boldsymbol{z}_\mathrm{r}) - \mathcal{T}(\boldsymbol{x}_1, \boldsymbol{z}_\mathrm{r})$ *the variance of the fluctuations is*

$$\mathrm{Var}\big(\Delta C_1^{(1)}(\tau, \boldsymbol{x}_1, \boldsymbol{x}_2)\big) = \frac{\sigma_\mathrm{r}^2 l_\mathrm{r}^6 \sigma_\mathrm{s}^2 l_\mathrm{s}^3}{2^{15}\pi^7 c_0^5}\Big[\int \hat{F}_\varepsilon^2(\omega)\omega^6 \mathrm{d}\omega\Big] \frac{\rho^K_{\boldsymbol{x}_2,\boldsymbol{x}_1,\boldsymbol{z}_\mathrm{r}}}{|\boldsymbol{x}_1 - \boldsymbol{z}_\mathrm{r}|^2 |\boldsymbol{x}_2 - \boldsymbol{z}_\mathrm{r}|^2}.$$

In order to complete the picture we add that:
1) The coherence time of the fluctuations is the inverse of the bandwidth B of the noise sources.
2) The time lag-integrated variance is:

$$\begin{aligned}\int \mathrm{Var}\big(\Delta C_1^{(1)}(\tau, \boldsymbol{x}_1, \boldsymbol{x}_2)\big)\mathrm{d}\tau = \frac{\sigma_\mathrm{r}^2 l_\mathrm{r}^6 \sigma_\mathrm{s}^2 l_\mathrm{s}^3}{2^{15}\pi^7 c_0^6}\Big[\int \hat{F}_\varepsilon^2(\omega)\omega^6 \mathrm{d}\omega\Big] \int \mathrm{d}\boldsymbol{z} \frac{\rho(\boldsymbol{z})}{|\boldsymbol{z}_\mathrm{r} - \boldsymbol{z}|^2} \\ \times\Big(\frac{K^2_{\boldsymbol{z}_\mathrm{r},\boldsymbol{z}} + K^2_{\boldsymbol{z},\boldsymbol{z}_\mathrm{r}} + K^2_{\boldsymbol{z}_\mathrm{r},\boldsymbol{x}_1} + K^2_{\boldsymbol{z},\boldsymbol{x}_2} + K^2_{\boldsymbol{x}_2,\boldsymbol{z}}}{|\boldsymbol{x}_1 - \boldsymbol{z}_\mathrm{r}|^2 |\boldsymbol{x}_2 - \boldsymbol{z}|^2} \\ + \frac{K^2_{\boldsymbol{z}_\mathrm{r},\boldsymbol{z}} + K^2_{\boldsymbol{z},\boldsymbol{z}_\mathrm{r}} + K^2_{\boldsymbol{z}_\mathrm{r},\boldsymbol{x}_2} + K^2_{\boldsymbol{z},\boldsymbol{x}_1} + K^2_{\boldsymbol{x}_1,\boldsymbol{z}}}{|\boldsymbol{x}_1 - \boldsymbol{z}|^2 |\boldsymbol{x}_2 - \boldsymbol{z}_\mathrm{r}|^2}\Big).\end{aligned} \tag{45}$$

3) The quantity $\rho^K_{\boldsymbol{x}_1,\boldsymbol{x}_2,\boldsymbol{z}_\mathrm{r}}$ is the integral of the function $\boldsymbol{z} \to \rho(\boldsymbol{z})\big(K^2_{\boldsymbol{z}_\mathrm{r},\boldsymbol{z}} + K^2_{\boldsymbol{z}_\mathrm{r},\boldsymbol{x}_1}\big)$ over the surface $\mathcal{S}_{\boldsymbol{x}_1,\boldsymbol{x}_2,\boldsymbol{z}_\mathrm{r}}$ that has the form of an ellipsoid whose main axis is the line joining $\boldsymbol{z}_\mathrm{r}$ to $\boldsymbol{x}_2$. The support of this function is that of the scattering region. Therefore, the quantity $\rho^K_{\boldsymbol{x}_1,\boldsymbol{x}_2,\boldsymbol{z}_\mathrm{r}}$ is zero when the scattering region does not intersect the ellipsoid. The equation of the ellipsoid is

$$\mathcal{S}_{\boldsymbol{x}_1,\boldsymbol{x}_2,\boldsymbol{z}_\mathrm{r}} = \Big\{\boldsymbol{z} \text{ such that } |\boldsymbol{x}_2 - \boldsymbol{z}| + |\boldsymbol{z}_\mathrm{r} - \boldsymbol{z}| = 2|\boldsymbol{x}_1 - \boldsymbol{z}_\mathrm{r}| + |\boldsymbol{x}_2 - \boldsymbol{z}_\mathrm{r}|\Big\}.$$

If the sensor array is centered at $\boldsymbol{x}_0$ and the diameter of the array is smaller than the distance from the array to the reflector, then the ellipsoid is an oblate spheroid centered at $\boldsymbol{x}_c = (\boldsymbol{z}_\mathrm{r} + \boldsymbol{x}_0)/2$, its main axis is the line from $\boldsymbol{z}_\mathrm{r}$ to $\boldsymbol{x}_0$, the polar radius is $(3/2)|\boldsymbol{z}_\mathrm{r} - \boldsymbol{x}_0|$ and the equatorial radius is $\sqrt{2}|\boldsymbol{z}_\mathrm{r} - \boldsymbol{x}_0|$ (see Figure 5):

$$\mathcal{S}_{\boldsymbol{z}_\mathrm{r}} = \Big\{\boldsymbol{z} \text{ such that } |\boldsymbol{z} - \boldsymbol{x}_0| + |\boldsymbol{z} - \boldsymbol{z}_\mathrm{r}| = 3|\boldsymbol{x}_0 - \boldsymbol{z}_\mathrm{r}|\Big\}. \tag{46}$$

The following proposition is proved in Appendix B. It describes the first moment of cross correlation $\Delta C_2^{(1)}$. It is in this result that the second order term $\hat{G}_2$ in (36) turns out not to make a significant contribution, as noted at the end of the previous section.

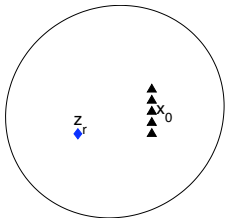

FIGURE 5. The ellipsoid $\mathcal{S}_{\boldsymbol{z}_{\rm r}}$ defined by (46) which determines the scattering region giving rise to fluctuations in the cross correlation at lag time equal to the sum of travel times.

Proposition 4. *The mean of the cross correlation $\Delta C_2^{(1)}$ has a singular contribution at lag time equal to the sum of travel times $\mathcal{T}(\boldsymbol{x}_2,\boldsymbol{z}_{\rm r})+\mathcal{T}(\boldsymbol{x}_1,\boldsymbol{z}_{\rm r})$ provided that the ray going from $\boldsymbol{z}_{\rm r}$ to $\boldsymbol{x}_1$ reaches into the scattering region behind the sensors (see the left picture in Figure 6). This singular contribution has the form*

(47)
$$\mathbb{E}\big[\Delta C_2^{(1)}\big(\tau,\boldsymbol{x}_1,\boldsymbol{x}_2\big)\big]=\frac{\sigma_{\rm r} l_{\rm r}^3\sigma_{\rm s}^2 l_{\rm s}^3}{2^9\pi^4 c_0^5}\frac{K^\rho_{\boldsymbol{x}_1,\boldsymbol{z}_{\rm r}}}{|\boldsymbol{z}_{\rm r}-\boldsymbol{x}_1||\boldsymbol{z}_{\rm r}-\boldsymbol{x}_2|}\partial_\tau^5 F_\varepsilon\big(\tau-[\mathcal{T}(\boldsymbol{x}_2,\boldsymbol{z}_{\rm r})+\mathcal{T}(\boldsymbol{x}_1,\boldsymbol{z}_{\rm r})]\big),$$

where

(48)
$$K^\rho_{\boldsymbol{x},\boldsymbol{z}}=\int_0^\infty K^\rho\Big(\boldsymbol{x}+\frac{\boldsymbol{x}-\boldsymbol{z}}{|\boldsymbol{x}-\boldsymbol{z}|}l\Big)\mathrm{d}l,\qquad K^\rho(\boldsymbol{y})=\rho(\boldsymbol{y})\int\frac{K(\boldsymbol{y}')}{|\boldsymbol{y}-\boldsymbol{y}'|^2}\mathrm{d}\boldsymbol{y}'.$$

The mean of the cross correlation $\Delta C_2^{(1)}$ has a singular contribution at lag time equal to minus the sum of travel times $\mathcal{T}(\boldsymbol{x}_2,\boldsymbol{z}_{\rm r})+\mathcal{T}(\boldsymbol{x}_1,\boldsymbol{z}_{\rm r})$ provided that the ray going from $\boldsymbol{z}_{\rm r}$ to $\boldsymbol{x}_2$ reaches into the scattering region behind the sensors (see the right picture in Figure 6):

(49)
$$\begin{aligned}&\mathbb{E}\big[\Delta C_2^{(1)}\big(\tau,\boldsymbol{x}_1,\boldsymbol{x}_2\big)\big]\\&=-\frac{\sigma_{\rm r} l_{\rm r}^3\sigma_{\rm s}^2 l_{\rm s}^3}{2^9\pi^4 c_0^5}\frac{K^\rho_{\boldsymbol{x}_2,\boldsymbol{z}_{\rm r}}}{|\boldsymbol{z}_{\rm r}-\boldsymbol{x}_1||\boldsymbol{z}_{\rm r}-\boldsymbol{x}_2|}\partial_\tau^5 F_\varepsilon\big(\tau+[\mathcal{T}(\boldsymbol{x}_2,\boldsymbol{z}_{\rm r})+\mathcal{T}(\boldsymbol{x}_1,\boldsymbol{z}_{\rm r})]\big).\end{aligned}$$

The variance of the fluctuations of $\Delta C_2^{(1)}$ is smaller (of order $O(\sigma_{\rm r}^2\sigma_{\rm s}^4)$) than the variance of $\Delta C_1^{(1)}$ (of order $O(\sigma_{\rm r}^2\sigma_{\rm s}^2)$ as seen in Proposition 3) so we shall not describe it in detail.

4.6. **The cross correlation at the difference of travel times.** We can now describe the form of the cross correlation at lag time equal to the difference of travel times, which consists of a singular peak generated by the primary energy flux and described in Proposition 2, and random fluctuations described in Proposition 3.

The order of magnitude of the height of the singular peak can be obtained from (17). If we denote by $d(A,R)$ the distance from the source array to the reflector, by W_K the width of the source region, by K_0 the typical value of K, and by B the bandwidth of the noise sources, then (17) shows that the typical height (amplitude) of the singular peak is

(50)
$$\Delta C_0^{(1)}\sim\frac{\sigma_{\rm r} l_{\rm r}^3 W_K K_0}{c_0 d(A,R)^2}\Big[\int|\omega|\hat{F}_\varepsilon(\omega)\mathrm{d}\omega\Big]$$

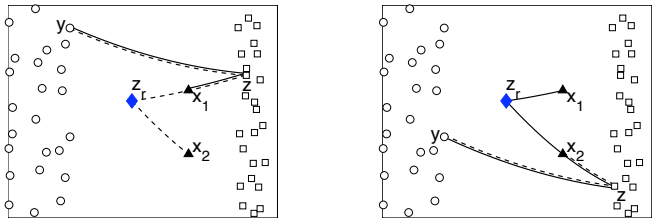

FIGURE 6. Configurations of ray segments that contribute to singular components of the differential cross correlation $\Delta C_2^{(1)}$ of signals between $\boldsymbol{x}_1$ and $\boldsymbol{x}_2$ in the presence of the reflector at $\boldsymbol{z}_{\rm r}$. The circles are noise sources, the triangles are sensors, the squares are scatterers, and the diamond is the reflector. The scatterers provide secondary daylight illumination and give rise to a singular component at lag time equal to (plus or minus) the sum of travel times $\mathcal{T}(\boldsymbol{x}_1, \boldsymbol{z}_{\rm r}) + \mathcal{T}(\boldsymbol{x}_2, \boldsymbol{z}_{\rm r})$.

and the width of the peak in time lag τ is of order B^{-1}. If we denote by ω_0 the central frequency of the sources then the height of the peak is

$$\Delta C_0^{(1)} \sim \frac{\sigma_{\rm r} l_{\rm r}^3 W_K K_0 \omega_0}{c_0 d(A,R)^2}. \tag{51}$$

It is possible to give the order of magnitude of the variance of the fluctuations of the cross correlation at lag time equal to the difference of travel times from (42). This order of magnitude depends on the location of the scattering region. Indeed we can observe the following important fact:

> The variance (42) of the fluctuations of the cross correlation at lag time equal to the difference of travel times depends only on the scatterers localized along the rays that contribute to the singular peak at the difference of travel times and shown in Figure 2c-d, to leading order.

The variance is especially sensitive to the scatterers close to the reflector at $\boldsymbol{z}_{\rm r}$ and close to the sensor array, as can be seen from the form of the denominators in (42).

We consider two typical situations:

- if there are scatterers only to the right of the sensor array, as in Figure 7a, then these scatterers do not produce fluctuations in the cross correlation at the difference of travel times. The singular contribution at this lag time is thus not affected, and the backlight imaging functional will have a clear but elongated peak at the reflector location.

- if there are scatterers only between the sources and the reflector, then there are fluctuations in the cross correlation at lag time equal to the difference of travel times. If we denote by $d(A,R)$ the distance from the sensor array to the reflector, by $d^-(A,S)$ the distance from the sensor array to the scattering region that is between the sources and the reflector, by W_K the width of the source region, by $W_{\rm s}^-$ the width of the scattering region that is between the sources and the reflector, then

we have

$$\mathrm{Std}\big(\Delta C_1^{(1)}\big) \sim \frac{\sigma_{\rm r} l_{\rm r}^3 \sigma_{\rm s} l_{\rm s}^{3/2}}{c_0^{5/2}} \Big[\int \hat{F}_\varepsilon^2(\omega)\omega^6 \mathrm{d}\omega \Big]^{1/2} \frac{K_0 W_K (W_{\rm s}^-)^{1/2}}{d(A,R)^{3/2} d^-(A,S)}. \tag{52}$$

If we denote by B the bandwidth of the noise sources and by ω_0 the central frequency, then the SNR of the main peak at the difference of travel times $\mathcal{T}(\boldsymbol{x}_1,\boldsymbol{z}_{\rm r}) - \mathcal{T}(\boldsymbol{z}_1,\boldsymbol{z}_{\rm r})$ over the standard deviation of the fluctuations of the cross correlations at this lag time is

$$\frac{\Delta C_0^{(1)}}{\mathrm{Std}\big(\Delta C_1^{(1)}\big)} \sim \frac{c_0^{3/2}}{\sigma_{\rm s} l_{\rm s}^{3/2}} \frac{B^{1/2}}{\omega_0^2} \frac{d(A,S)}{(W_{\rm s}^-)^{1/2} d(A,R)^{1/2}}. \tag{53}$$

This formula gives an insight into the performance of cross correlation imaging in a scattering medium from the point of view of the SNR of the cross correlation at lag time equal to the difference of travel times, which has a singular contribution that influences the backlight imaging functional.

1) The SNR does not depend on the distance from the sensor array to the sources.

2) The SNR depends only on the scatterers localized along the rays that contribute to the singular peak at lag time equal to the difference of travel times and shown in Figure 2c-d.

3) The SNR depends on the distance from the sensor array to the reflector and it decays with this distance.

4) The SNR depends on the distance from the sensor array to the scattering region and it increases with this distance.

The noise sources have usually a large bandwidth, so it is possible to filter the recorded signals and to select a given frequency band of the form $[\omega_0 - B/2, \omega_0 + B/2]$ (with $B < \omega_0$). We can see that the resolution is proportional to B^{-1} while the SNR is proportional to $B^{1/2}$. By increasing the bandwidth, it is therefore possible to increase the SNR and to enhance the resolution.

When forming the imaging functional the cross correlations are summed as in (21). If we assume that the distances between the sensors are larger than c_0/B, then the cross correlations $\big(\Delta C_1^{(1)}(\tau,\boldsymbol{x}_j,\boldsymbol{x}_l)\big)_{j,l=1,\ldots,N}$ are uncorrelated from each other for all distinct pairs. Therefore the noise level is reduced by a factor $N/\sqrt{2}$ so that the SNR of the image is:

$$\frac{\mathbb{E}[\mathcal{I}]}{\mathrm{Std}(\mathcal{I})} \simeq \frac{N}{\sqrt{2}} \frac{\mathbb{E}\big[\Delta C^{(1)}\big]}{\mathrm{Std}\big(\Delta C^{(1)}\big)}. \tag{54}$$

This means that, even if the singular peaks of the cross correlations are buried by fluctuations due to the clutter, the imaging functional helps in building up the SNR.

4.7. **The cross correlation at the sum of travel times.** At a lag time equal to the sum of travel times $\mathcal{T}(\boldsymbol{x}_1,\boldsymbol{z}_{\rm r}) + \mathcal{T}(\boldsymbol{x}_2,\boldsymbol{z}_{\rm r})$, the cross correlation has a singular peak and random fluctuations. The width of the peak and the coherence time of the fluctuations are equal to B^{-1}. The order of magnitude of the height of the peak of the mean and of the standard deviation of the cross correlation at lag time equal to the sum of travel times is obtained from (47) and (43). The main result in this case is in the following remark:

> The mean (47) of the cross correlation has a singular contribution at lag time equal to the sum of travel times provided that the rays going from the reflector to the sensors intersect the scattering region.

The variance (43) of the fluctuations of the cross correlation at lag time equal to the sum of travel times depends only on the scatterers localized along the ellipsoid (46) to leading order.

If the scattering region intersects the rays going from the reflector to the sensors but is outside the region delimited by the ellipsoid (46), then the cross correlation exhibits a clear peak at the sum of travel times.

If the scattering region intersects the rays going from the reflector to the sensors and the ellipsoid (46), then we have the following. If we denote by $d(A,R)$ the distance from the sensor array to the reflector, by $d(A,S)$ the distance from the sensor array to the scattering region, by $d(K,S)$ the distance from the source region to the scattering region, by W_K the width of the source region, and by W_{s}^+ the width of the scattering region that is behind the sensor array, then we have

$$\mathbb{E}\big[\Delta C_2^{(1)}\big] \sim \frac{\sigma_{\mathrm{r}} l_{\mathrm{r}}^3 \sigma_{\mathrm{s}}^2 l_{\mathrm{s}}^3}{c_0^5} \frac{\mathrm{Vol}(\Omega_K) W_{\mathrm{s}}^+ K_0}{d(K,S)^2 d(A,R)^2} \Big[\int \hat{F}_\varepsilon(\omega) |\omega|^5 \mathrm{d}\omega \Big], \tag{55}$$

$$\mathrm{Std}\big(\Delta C_1^{(1)}\big) \sim \frac{\sigma_{\mathrm{r}} l_{\mathrm{r}}^3 \sigma_{\mathrm{s}} l_{\mathrm{s}}^{3/2}}{c_0^{5/2}} \Big[\int \hat{F}_\varepsilon^2(\omega) \omega^6 \mathrm{d}\omega \Big]^{1/2} \frac{W_K W_{\mathrm{s}}^+ K_0}{d(A,R)^3}. \tag{56}$$

The SNR of the main peak at the sum of travel times $\mathcal{T}(\boldsymbol{x}_1, \boldsymbol{z}_{\mathrm{r}}) + \mathcal{T}(\boldsymbol{z}_1, \boldsymbol{z}_{\mathrm{r}})$ over the standard deviation of the fluctuations of the cross correlations at this lag time is

$$\frac{\mathbb{E}\big[\Delta C_2^{(1)}\big]}{\mathrm{Std}\big(\Delta C_1^{(1)}\big)} \sim \frac{\sigma_{\mathrm{s}} l_{\mathrm{s}}^{3/2}}{c_0^{5/2}} \omega_0^2 B^{1/2} \frac{\mathrm{Vol}(\Omega_K) d(A,R)}{W_K d(K,S)^2}. \tag{57}$$

Let us discuss the main properties of the SNR of the cross correlation at lag time equal to the sum of travel times:
1) The SNR is high if the scattering region is far enough from the sensor array (more exactly, if it is outside the volume delimited by the ellipsoid (46)).
2) It is sensitive to the scattering region behind the sensor array when not too far.
3) It increases with the source volume but decays with the square distance from the source region to the scattering region.
4) It increases with the bandwidth. This shows that both the resolution and the SNR increases with the bandwidth.

Note that the third point simply means that the SNR is proportional to the energy emitted by the noise sources and received by the scattering region, which is then scattered to provide the secondary daylight illumination. The SNR of the image is given by the same expression (54) as in the difference travel time case of the previous section.

4.8. **On the trade-off between resolution enhancement and signal-to-noise ratio reduction.** We can now discuss the trade-off between resolution enhancement and SNR reduction due to scattering.

1) Proposition 4 shows that scattering leads to the appearance of a singular contribution in the cross correlation at lag time equal to (plus or minus) the sum of travel times. This happens provided there are rays issuing from the scattering region and going to the sensors and then to the reflector. The scatterers can thus be seen as secondary sources that could provide a daylight illumination for the reflector, as shown in Figure 6. This ensures that the daylight imaging functional (21) will have a peak at the reflector location with good range resolution. This is a very interesting result, the one we wanted to get in this paper, because in the backlight illumination configuration considered here the direct waves do not generate such a

peak and only the backlight imaging functional (22) can be used in the absence of scattering, which produces an elongated peak with poor range resolution.

2) Proposition 3 shows that the scattered waves generate additional fluctuations in the cross correlations that can be larger than the additional peaks considered in Proposition 4. As a consequence, the peak in the daylight imaging functional (21) at the reflector location that we have just mentioned can be buried in the contributions of the non-singular random components. This happens in the case shown in the schematic of Figure 12, which we discuss in Subsection 6.2.

3) There exist special configurations which are favorable for imaging with secondary illumination from scatterers. If the scatterers are far enough from the sensor array, in the sense that the scattering region is outside the region delimited by the ellipsoid (46), then the fluctuations of the cross correlation at lag time equal to the sum of travel times are small. This situation does not prevent the existence of a ray going through the reflector, a sensor, and a scatterer, which ensures the existence of a singular peak in the cross correlation at lag time equal to the sum of travel times.

4) What happens if these favorable conditions are not met? We will see in Section 6 that an iterated cross correlation technique can often enhance the contributions of the scattered waves in order to strengthen the singular components of the scattered waves and improve the SNR of the image.

4.9. **Numerical simulation of migration imaging with cross correlations in the presence of scatterers.** In the previous subsection we saw that the scatterers can play the role of secondary sources. Here we illustrate this fact by showing that it is possible to use the daylight imaging functional (21) in configurations that are not in a daylight illumination configuration without the scattering.

In Figure 7 we consider a configuration with a backlight illumination of the region of interest and with a layer of scattering medium behind it. We show the images obtained with the backlight imaging functional (22) and with the daylight imaging functional (21). The backlight imaging functional gives a good image (Figure 7b), as in Figure 3b, which is expected since it is the result of the contributions of the direct waves described in Proposition 2. More striking is the daylight imaging functional (Figure 7c) that also gives a good image, in contrast to Figure 3c. This shows that the layer of scattering medium succeeds in redirecting part of the flux of energy so that the region of interest experiences a secondary daylight illumination and the daylight imaging functional gives a good image. By comparing with the primary daylight configuration of Figure 4, one can see that the daylight imaging functional in Figure 7c has range and cross-range resolutions that are comparable to the ones obtained in a primary daylight configuration. Here the situation is favorable in that the scattering region does not intersect the ellipsoid (46), so that the fluctuations of the cross correlation at lag time equal to the sum of travel times are small and the SNR of the image in Figure 7c is high. A lower SNR can become problematic if the scattering region intersects the ellipsoid (46). We will see in Section 6 how to enhance the contributions of the scattered waves by an iterative cross correlation technique and thus increase the SNR of the image.

5. **Passive sensor imaging with a reflecting interface.** In this section we consider the case in which scattering is not generated by random inhomogeneities but by a partially or totally reflecting interface in the medium. This configuration

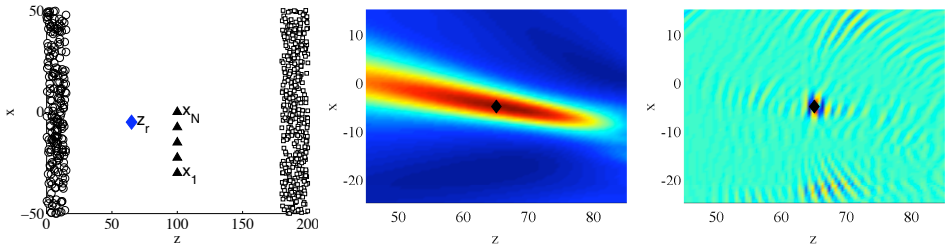

a) Configuration **b)** $\mathcal{I}^{\mathrm{B}}$ **c)** $\mathcal{I}^{\mathrm{D}}$

FIGURE 7. Passive sensor imaging using the differential cross correlation technique in a scattering medium. The backlight illumination configuration is shown in Figure a: the circles are the noise sources, the triangles are the sensors, the diamond is the reflector, and the squares are the scatterers. Figure b shows the image obtained with the backlight imaging functional (22). Figure c shows the image obtained with the daylight imaging functional (21).

is of interest in geophysical applications where the earth's surface may play the role of a reflecting interface.

5.1. **Stationary phase analysis of the cross correlation with a reflecting interface.** In this section we will assume that the medium is homogeneous with background speed c_0 and the interface I_{m} is a plane of equation $x_3 = z_{\mathrm{m}}$. As a consequence the method of images can be applied. For any point $\boldsymbol{x} = (x_1, x_2, x_3)$ we associate the virtual point $\tilde{\boldsymbol{x}}$ which is the image of $\boldsymbol{x}$ through the symmetry with respect to the plane I_{m}:

$$\tilde{\boldsymbol{x}} = (x_1, x_2, 2z_{\mathrm{m}} - x_3).$$

The Green's function in the presence of the reflecting interface and in the absence of the reflector is then simply

$$\hat{G}_{\mathrm{m}}(\omega, \boldsymbol{x}, \boldsymbol{y}) = \hat{G}_0(\omega, \boldsymbol{x}, \boldsymbol{y}) + R_{\mathrm{m}}\hat{G}_0(\omega, \boldsymbol{x}, \tilde{\boldsymbol{y}}),$$

with R_{m} the reflection coefficient of the interface and $\hat{G}_0$ the free space Green's function (14). In the case of a perfect mirror we have $R_{\mathrm{m}} = -1$. In the presence of the reflector at $\boldsymbol{z}_{\mathrm{r}}$ and in the point interaction approximation for the reflector, the Green's function is of the form

$$\hat{G}_{\mathrm{m,r}}(\omega, \boldsymbol{x}, \boldsymbol{y}) = \hat{G}_{\mathrm{m}}(\omega, \boldsymbol{x}, \boldsymbol{y}) + \frac{\omega^2}{c_0^2}\sigma_{\mathrm{r}} l_{\mathrm{r}}^3 \hat{G}_{\mathrm{m}}(\omega, \boldsymbol{x}, \boldsymbol{z}_{\mathrm{r}})\hat{G}_{\mathrm{m}}(\omega, \boldsymbol{z}_{\mathrm{r}}, \boldsymbol{y}),$$

and it contains the contributions of rays reflected by the interface.

In the next proposition 5, proved in Appendix C, the virtual source region denotes the image of the support of the function K through the symmetry with respect to the plane I_{m}. Proposition 5 shows that the mirror generates virtual sources which play the role of secondary noise sources and can provide a daylight illumination of the region of interest (the reflector and the sensors). Beyond the interesting additional singular components described below, at lag times equal to plus or minus the sum of travel times that contribute to the daylight imaging functional, there are additional components at lag times which are at least of the order of twice the travel time

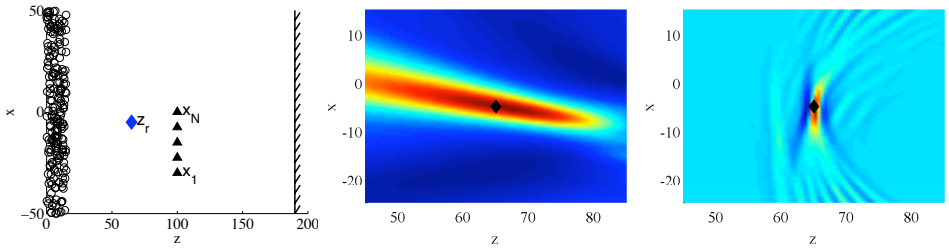

a) Configuration **b)** $\mathcal{I}^{\mathrm{B}}$ **c)** $\mathcal{I}^{\mathrm{D}}$

FIGURE 8. Passive sensor imaging using the differential cross correlation technique in a homogeneous medium with a reflecting boundary. The configuration is shown in Figure a: the circles are the noise sources, the triangles are the sensors, and the diamond is the reflector. Figure b shows the image obtained with the backlight imaging functional (22). Figure c shows the image obtained with the daylight imaging functional (21).

from the sensors to the reflecting interface, so that they do not play any role in the daylight imaging functional provided the reflecting interface is distant enough.

Proposition 5. *Let us consider the backlight illumination configuration with a mirror behind the sensor array (Figure 8a). The differential cross correlation has several singular components.*

There is a singular contribution at lag time equal to the difference of travel times as described by (17).

There is a singular contribution at lag time equal to the sum of travel times $\mathcal{T}(\boldsymbol{x}_2,\boldsymbol{z}_{\mathrm{r}})+\mathcal{T}(\boldsymbol{x}_1,\boldsymbol{z}_{\mathrm{r}})$ *which has the form:*

(58)
$$\Delta C^{(1)}(\tau,\boldsymbol{x}_1,\boldsymbol{x}_2)=\frac{\sigma_{\mathrm{r}} l_{\mathrm{r}}^3 R_{\mathrm{m}}^2}{32\pi^2 c_0}\frac{\widetilde{K}_{\boldsymbol{x}_1,\boldsymbol{z}_{\mathrm{r}}}}{|\boldsymbol{z}_{\mathrm{r}}-\boldsymbol{x}_1||\boldsymbol{z}_{\mathrm{r}}-\boldsymbol{x}_2|}\partial_\tau F_\varepsilon\big(\tau-[\mathcal{T}(\boldsymbol{x}_2,\boldsymbol{z}_{\mathrm{r}})+\mathcal{T}(\boldsymbol{x}_1,\boldsymbol{z}_{\mathrm{r}})]\big),$$

there is a singular contribution at lag time equal to minus the sum of travel times $-[\mathcal{T}(\boldsymbol{x}_2,\boldsymbol{z}_{\mathrm{r}})+\mathcal{T}(\boldsymbol{x}_1,\boldsymbol{z}_{\mathrm{r}})]$ *which has the form:*

(59)
$$\Delta C^{(1)}(\tau,\boldsymbol{x}_1,\boldsymbol{x}_2)=-\frac{\sigma_{\mathrm{r}} l_{\mathrm{r}}^3 R_{\mathrm{m}}^2}{32\pi^2 c_0}\frac{\widetilde{K}_{\boldsymbol{x}_2,\boldsymbol{z}_{\mathrm{r}}}}{|\boldsymbol{z}_{\mathrm{r}}-\boldsymbol{x}_1||\boldsymbol{z}_{\mathrm{r}}-\boldsymbol{x}_2|}\partial_\tau F_\varepsilon\big(\tau+[\mathcal{T}(\boldsymbol{x}_2,\boldsymbol{z}_{\mathrm{r}})+\mathcal{T}(\boldsymbol{x}_1,\boldsymbol{z}_{\mathrm{r}})]\big),$$

where $\widetilde{K}_{\boldsymbol{x},\boldsymbol{z}}$ *is the energy released by the virtual sources along the ray joining* $\boldsymbol{x}$ *and* $\boldsymbol{z}$*:*

(60)
$$\widetilde{K}_{\boldsymbol{x},\boldsymbol{z}}=\int_0^\infty \widetilde{K}\Big(\boldsymbol{x}+\frac{\boldsymbol{x}-\boldsymbol{z}}{|\boldsymbol{x}-\boldsymbol{z}|}l\Big)\mathrm{d}l,\qquad \widetilde{K}(\boldsymbol{y})=K(\widetilde{\boldsymbol{y}}).$$

Note that $\widetilde{K}_{\boldsymbol{x}_j,\boldsymbol{z}_{\mathrm{r}}}$ is positive only when the ray going from $\boldsymbol{z}_{\mathrm{r}}$ to $\boldsymbol{x}_j$ extends into the virtual source region, which is the secondary daylight illumination configuration mentioned above.

5.2. **Numerical simulations of migration imaging with cross correlations in presence of an interface.** In Figure 8 we show the images obtained in a backlight illumination configuration with a mirror behind the region of interest.

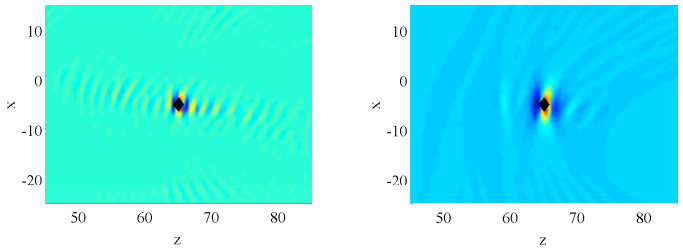

a) $\mathcal{I}^{\mathrm{B}} \times \mathcal{I}^{\mathrm{D}}$, scattering layer **b)** $\mathcal{I}^{\mathrm{B}} \times \mathcal{I}^{\mathrm{D}}$, reflecting boundary

Figure 9. Images obtained by multiplying the backlight imaging functional (22) with the daylight imaging functional (21). Picture a corresponds to the configuration with a scattering layer of Figure 7a and picture b corresponds to the configuration with a reflecting boundary of Figure 8a.

The image obtained with the backlight imaging functional (22) is expected since it is the result of the contributions of the direct waves described in Proposition 2. The good image obtained with the daylight imaging functional (21) illustrates the theoretical predictions of Proposition 5: the mirror generates virtual sources that illuminate the region of interest with a secondary daylight illumination.

The configuration with a mirror and the configuration with a randomly scattering medium studied in the previous section have therefore common points: They both provide a secondary daylight illumination. As a result, the daylight migration functional can use the scattered or reflected waves and gives a good range resolution of the reflector, while the backlight migration functional uses the direct waves and gives a good cross range resolution of the reflector. By multiplying the two functionals, one obtains the location of the reflector with a good accuracy (see Figure 9).

There are two major differences between the configuration with a mirror and the configuration with a randomly scattering medium:
1) A very significant part of the energy flux is reflected in the case of the mirror, while only a small part is scattered in the case of a randomly scattering medium (in the weakly scattering regime that we address).
2) The randomly scattering medium redirects the energy flux in all directions, while the reflecting interface redirects the energy flux only in the specular direction.

This means that the mirror induces an enhancement of the directional diversity that is strong but only in a special direction. Therefore the enhancement of the directional diversity by a mirror is not as effective as the one provided by a randomly scattering medium. If the orientation of the interface is not adjusted properly, so that there is no ray issuing from a virtual source point and going to a sensor and to the reflector, then the daylight imaging functional does not perform well as predicted by Proposition 5 and as shown in Figure 10. In contrast to this result, the orientation of the randomly scattering layer plays no role, as predicted by Proposition 3 and as shown in Figure 11.

6. **Iterated cross correlations for passive imaging in a randomly scattering medium.** We have noted in Section 4 that the peaks in the differential cross

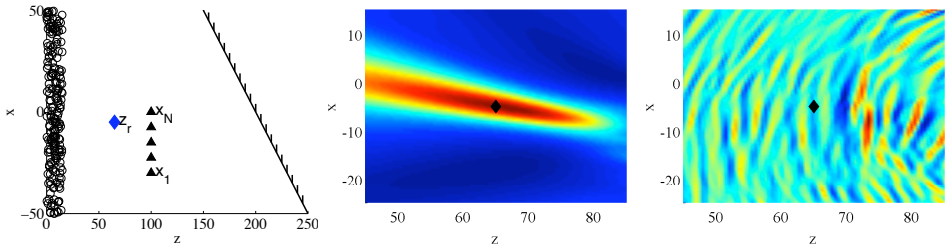

a) Configuration **b)** $\mathcal{I}^{\mathrm{B}}$ **c)** $\mathcal{I}^{\mathrm{D}}$

FIGURE 10. Passive sensor imaging using the differential cross correlation technique in a homogeneous medium with an oblique reflecting boundary (the angle is $\pi/4$, which means that the right-going primary energy flux is reflected as a down-going energy flux). The configuration is shown in Figure a. Figure b shows the image obtained with the backlight imaging functional (22). Figure c shows the image obtained with the daylight imaging functional (21).

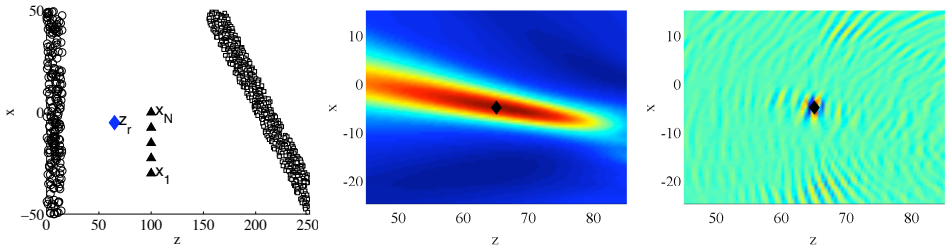

a) Configuration **b)** $\mathcal{I}^{\mathrm{B}}$ **c)** $\mathcal{I}^{\mathrm{D}}$

FIGURE 11. Passive sensor imaging using the differential cross correlation technique in a homogeneous medium with an oblique randomly scattering layer. The configuration is shown in Figure a. Figure b shows the image obtained with the backlight imaging functional (22). Figure c shows the image obtained with the daylight imaging functional (21).

correlation $\Delta C^{(1)}(\tau, \boldsymbol{x}_j, \boldsymbol{x}_l)$ that are relevant to imaging of reflectors can be buried in fluctuations. This happens when the SNR of the peaks at lag time equal to plus or minus the sum of travel times $\pm[\mathcal{T}(\boldsymbol{x}_j, \boldsymbol{z}_{\mathrm{r}}) + \mathcal{T}(\boldsymbol{x}_l, \boldsymbol{z}_{\mathrm{r}})]$ is low. In this section we introduce an iterated cross correlation imaging technique that masks the contributions of the direct waves and increases the effective SNR of the peaks. This technique was shown to be efficient for inter-sensor travel time estimation in [13, 26] and is briefly reviewed in Appendix D. In the next subsections we describe this approach for reflector imaging with secondary daylight illumination from scattering, and present the results of some numerical simulations.

6.1. **The coda cross correlation.** It is possible to form a special fourth-order differential cross correlation matrix $\Delta C_T^{(3)}(\tau, \boldsymbol{x}_j, \boldsymbol{x}_l)$ between sensors $(\boldsymbol{x}_j)_{j=1,\ldots,N}$

from the differential cross correlations $\Delta C_T(\tau, \boldsymbol{x}_j, \boldsymbol{x}_l)$ obtained from the recorded data. This is done as follows.

1) Calculate the coda (i.e. the tails) by truncation of the differential cross correlations:

$$\Delta C_{T,\mathrm{coda}}(\tau, \boldsymbol{x}_j, \boldsymbol{x}_l) = \Delta C_T(\tau, \boldsymbol{x}_j, \boldsymbol{x}_l)\mathbf{1}_{[T_{\mathrm{c}1}, T_{\mathrm{c}2}]}(|\tau|), \qquad j, l = 1, \ldots, N.$$

2) Cross correlate the tails of the differential cross correlations and sum them over all complementary sensors in the array to form the coda cross correlation between $\boldsymbol{x}_j$ and $\boldsymbol{x}_l$:

(61)
$$\Delta C_T^{(3)}(\tau, \boldsymbol{x}_j, \boldsymbol{x}_l) = \sum_{k=1, k\notin\{j,l\}}^{N} \int \Delta C_{T,\mathrm{coda}}(\tau', \boldsymbol{x}_k, \boldsymbol{x}_j)\Delta C_{T,\mathrm{coda}}(\tau' + \tau, \boldsymbol{x}_k, \boldsymbol{x}_l)\mathrm{d}\tau'.$$

This algorithm depends on three important time parameters:

1) The time T is the integration time and it should be large so as to ensure statistical stability with respect to the distribution of the noise sources.

2) The time $T_{\mathrm{c}1}$ is chosen so that the parts of the Green's functions $t \mapsto G(t, \boldsymbol{x}_k, \boldsymbol{x}_j)$ and $t \mapsto G(t, \boldsymbol{x}_k, \boldsymbol{x}_l)$ limited to $[T_{\mathrm{c}1}, T_{\mathrm{c}2}]$ do not contain the contributions of the direct waves. This means that $T_{\mathrm{c}1}$ depends on the index of the sensors j, l, k and should be a little bit larger than $\max(\mathcal{T}(\boldsymbol{x}_k, \boldsymbol{x}_j), \mathcal{T}(\boldsymbol{x}_k, \boldsymbol{x}_l))$.

3) The time $T_{\mathrm{c}2}$ should be large enough so that the parts of the Green's functions $t \mapsto G(t, \boldsymbol{x}_k, \boldsymbol{x}_j)$ and $t \mapsto G(t, \boldsymbol{x}_k, \boldsymbol{x}_l)$ limited to $[T_{\mathrm{c}1}, T_{\mathrm{c}2}]$ contain the contributions of the incoherent scattered waves. This means that $T_{\mathrm{c}2}$ should be of the order of the power delay spread.

As shown in [13], it follows from the statistical stability of the cross correlation C_T that the differential coda cross correlation $\Delta C_T^{(3)}$ is a self-averaging quantity and it is equal to the statistical differential coda cross correlation $\Delta C^{(3)}$ as $T \to \infty$:

$$\Delta C^{(3)}(\tau, \boldsymbol{x}_j, \boldsymbol{x}_l) = \sum_{k=1, k\notin\{j,l\}}^{N} \int \overline{\Delta \hat{C}^{(1)}_{\mathrm{coda}}}(\omega, \boldsymbol{x}_k, \boldsymbol{x}_j)\Delta \hat{C}^{(1)}_{\mathrm{coda}}(\omega, \boldsymbol{x}_k, \boldsymbol{x}_l)e^{-i\omega\tau}\mathrm{d}\omega,$$

$$\Delta C^{(1)}_{\mathrm{coda}}(\tau, \boldsymbol{x}_k, \boldsymbol{x}_l) = \Delta C^{(1)}(\tau, \boldsymbol{x}_k, \boldsymbol{x}_l)\mathbf{1}_{[T_{\mathrm{c}1}, T_{\mathrm{c}2}]}(|\tau|).$$

The time windowing is important because it selects the contributions that we want to use for imaging the reflector at $\boldsymbol{z}_{\mathrm{r}}$. The asymptotic analysis of the functional $\Delta C^{(3)}$ can be carried out under the same conditions and with the same tools as those used in Section 4. This involves some long and tedious calculations that have not been carried out at present. However we do know that the differential coda cross correlation $\Delta C^{(3)}$ has singular components at lag time equal to (plus or minus) the sum of travel times $\pm[\mathcal{T}(\boldsymbol{x}_1, \boldsymbol{z}_{\mathrm{r}}) + \mathcal{T}(\boldsymbol{x}_2, \boldsymbol{z}_{\mathrm{r}})]$, and has fewer additional terms than the usual differential cross correlation studied in Subsection 4.2. As a consequence we expect that migration of the differential coda cross correlation using the daylight migration functional will produce an image of the reflector with a higher SNR.

An alternative version of the differential coda cross correlation can be obtained with the following algorithm:

1) Calculate the tails of the cross correlations $C_{T,\mathrm{coda}}$ using the data C_T collected in the presence of the reflector and the tails of the cross correlations $C_{T,\mathrm{coda},0}$ using

the data $C_{T,0}$ collected in its absence:

$$C_{T,\mathrm{coda}}(\tau,\boldsymbol{x}_j,\boldsymbol{x}_l)=C_T(\tau,\boldsymbol{x}_j,\boldsymbol{x}_l)\mathbf{1}_{[T_{\mathrm{c}1},T_{\mathrm{c}2}]}(|\tau|),\qquad j,l=1,\ldots,N,$$
$$C_{T,\mathrm{coda},0}(\tau,\boldsymbol{x}_j,\boldsymbol{x}_l)=C_{T,0}(\tau,\boldsymbol{x}_j,\boldsymbol{x}_l)\mathbf{1}_{[T_{\mathrm{c}1},T_{\mathrm{c}2}]}(|\tau|),\qquad j,l=1,\ldots,N.$$

2) Compute the coda cross correlations $C_T^{(3)}$ using $C_{T,\mathrm{coda}}$ and $C_{T,0}^{(3)}$ using $C_{T,\mathrm{coda},0}$:

$$C_T^{(3)}(\tau,\boldsymbol{x}_j,\boldsymbol{x}_l)=\sum_{k=1,k\notin\{j,l\}}^{N}\int C_{T,\mathrm{coda}}(\tau',\boldsymbol{x}_k,\boldsymbol{x}_j)C_{T,\mathrm{coda}}(\tau'+\tau,\boldsymbol{x}_k,\boldsymbol{x}_l)\mathrm{d}\tau',$$
$$C_{T,0}^{(3)}(\tau,\boldsymbol{x}_j,\boldsymbol{x}_l)=\sum_{k=1,k\notin\{j,l\}}^{N}\int C_{T,\mathrm{coda},0}(\tau',\boldsymbol{x}_k,\boldsymbol{x}_j)C_{T,\mathrm{coda},0}(\tau'+\tau,\boldsymbol{x}_k,\boldsymbol{x}_l)\mathrm{d}\tau'.$$

3) Take the difference between the coda cross correlations:

$$\Delta C_T^{(4)}(\tau,\boldsymbol{x}_j,\boldsymbol{x}_l)=C_T^{(3)}(\tau,\boldsymbol{x}_j,\boldsymbol{x}_l)-C_{T,0}^{(3)}(\tau,\boldsymbol{x}_j,\boldsymbol{x}_l),\qquad j,l=1,\ldots,N. \tag{62}$$

This algorithm produces a version $\Delta C_T^{(4)}$ of the differential coda cross correlation that is different from $\Delta C_T^{(3)}$. It is a statistically stable quantity. Its statistical average $\Delta C^{(4)}$ contains the singular components at lag time equal to (plus or minus) the sum of travel times $\pm[\mathcal{T}(\boldsymbol{x}_1,\boldsymbol{z}_{\mathrm{r}})+\mathcal{T}(\boldsymbol{x}_2,\boldsymbol{z}_{\mathrm{r}})]$ that we want to use for imaging and it has less unwanted contributions compared to $\Delta C^{(1)}$, similarly as $\Delta C^{3)}$. As a result we anticipate that both versions $\Delta C_T^{(3)}$ and $\Delta C_T^{(4)}$ of the differential coda cross correlation will produce images by migration.

6.2. **Numerical simulations of migration imaging with coda cross correlations.** In Figure 12 we consider a configuration in which the scattering region intersects the ellipsoid (46), which involves fluctuations of the cross correlation at lag time equal to the sum of travel times. As a result the daylight imaging functional with the usual differential cross correlation technique does not have a peak at the reflector location (Figure 12b), because the peaks at lag times equal to the sums of travel times $\pm[\mathcal{T}(\boldsymbol{x}_1,\boldsymbol{z}_{\mathrm{r}})+\mathcal{T}(\boldsymbol{x}_2,\boldsymbol{z}_{\mathrm{r}})]$ are obscured, contrary to what happens in Figure 7 when the scattering region does not intersect the ellipsoid. However, the daylight imaging functional with the differential coda cross correlation technique $\Delta C^{(3)}$ (figure 12e) or $\Delta C^{(4)}$ (figure 12h) gives a much better image. The overall result is that the backlight imaging functional $\mathcal{I}^{\mathrm{B}}$ using $\Delta C^{(1)}$ has good cross-range resolution and SNR while the daylight imaging functional $\mathcal{I}^{\mathrm{D}}$ using $\Delta C^{(3)}$ or $\Delta C^{(4)}$ has good range resolution and SNR. The multiplication of these two imaging functions gives the location of the reflector with greater accuracy (Figure 12f or i). The multiplication is a straightforward way to benefit from the advantages of both illuminations (direct and scattered) but it is probably not the optimal way. It can give a very good image in the presence of point-like reflectors but the image of an extended object may not be so good. This problem deserves more study.

7. **Conclusion.** In this paper we have analyzed the role of wave scattering in passive sensor imaging with ambient noise source illumination. The main result is a detailed quantitative analysis, presented in Section 4, of the trade-off between improved image resolution due to enhanced directional diversity of illumination by scattering versus lower signal-to-noise ratio (SNR) due to random fluctuations by scattering.

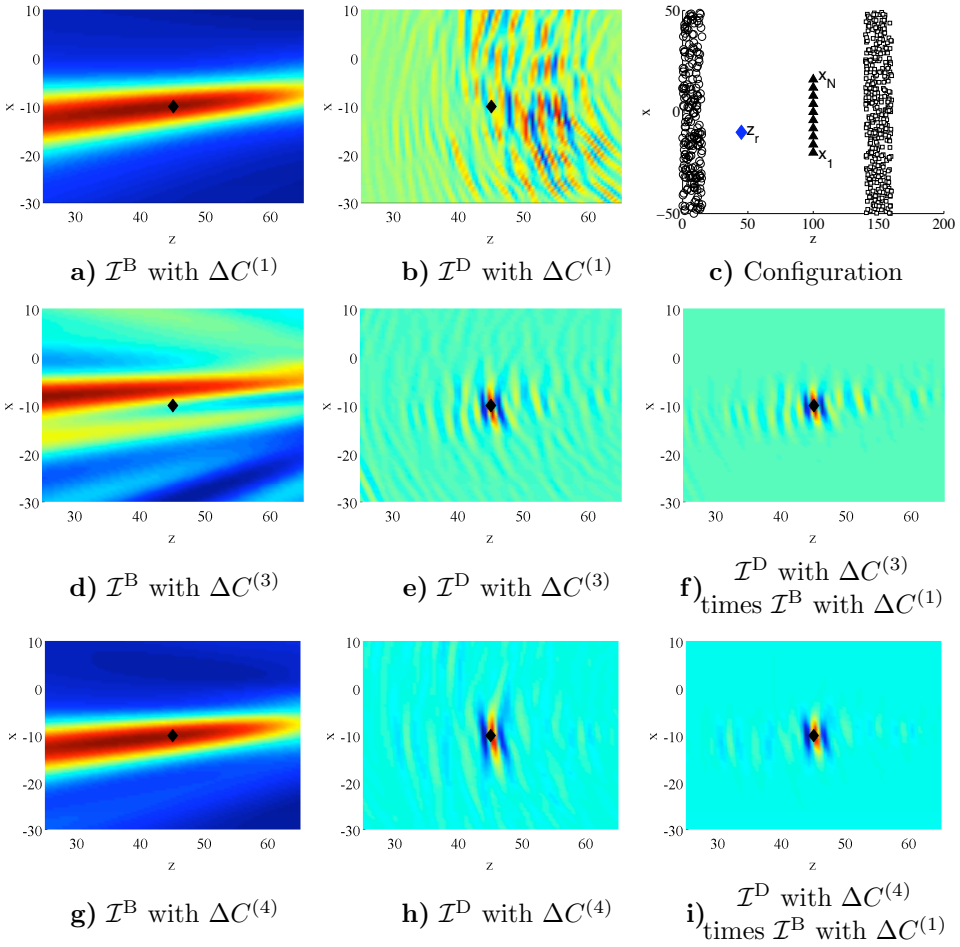

Figure 12. The configuration is shown in Figure c: the circles are the noise sources and the squares are the scatterers. Figure a (resp. b) shows the image obtained with the backlight imaging functional (22) (resp. the daylight imaging functional (21)) applied with the differential cross correlation $\Delta C^{(1)}$. Figure d (resp. e) shows the image obtained with the backlight imaging functional (22) (resp. the daylight imaging functional (21)) applied with the differential coda cross correlation $\Delta C^{(3)}$. Figure f shows the image obtained with the daylight imaging functional (21) applied with the differential coda cross correlation $\Delta C^{(3)}$ multiplied by the backlight imaging functional (22) applied with the differential cross correlation $\Delta C^{(1)}$. Figure g (resp. h) shows the image obtained with the backlight imaging functional (22) (the daylight imaging functional (21)) applied with the differential coda cross correlation $\Delta C^{(4)}$. Figure i shows the image obtained with the daylight imaging functional (21) applied with the differential coda cross correlation $\Delta C^{(4)}$ multiplied by the backlight imaging functional (22) applied with the differential cross correlation $\Delta C^{(1)}$.

One result is that a randomly scattering medium can increase the directional diversity of the energy flux that illuminates the region of interest consisting of the sensor array and the reflectors to be imaged. The range resolution can thus be enhanced significantly when the scattering medium provides a secondary daylight illumination for the region of interest, which generates a peak at the reflector location in the daylight imaging functional (21). We have also shown that a randomly scattering layer is more efficient for directional diversity enhancement than a deterministic reflecting surface.

A second result is that a randomly scattering medium also introduces random fluctuations in the cross correlations which reduce the SNR of the peaks in the cross correlations that contribute to the formation of the image. When the scattering region is far enough from the sensor array these fluctuations are small. When, however, the scattering region is close, the contribution of the reflectors to the peaks of the cross correlations can be weak compared to the standard deviation of the fluctuations due to the scattering. Migration (backpropagation) of the cross correlations then gives blurred and speckled images. We have also considered briefly the migration of special fourth-order cross correlations obtained by cross correlating the tails (coda) of the second-order cross correlations. This approach aims at masking the contributions of the direct waves and enhancing the contributions of the scattered waves. As a result, passive imaging using differential fourth-order coda cross correlations and a product of two different (backlight and daylight) migration functionals turns out to be quite effective in that it gives an image with good SNR and good resolution.

This trade-off between enhancement of the directional diversity of the illumination along with reduction of the SNR of the image makes sense only when the scattering is weak. As scattering strength increases migration of cross correlations, including fourth-order cross correlations, will eventually fail. It may be possible to estimate inter-sensor travel times, as was done in a recent study [7] in the microwave regime, in an indoor environment, using special statistical techniques, but it will be difficult to image in such strongly scattering media. Therefore, correlation based methods for passive sensor imaging in scattering media are likely to be effective in only regimes of weak to intermediate scattering.

Appendix A. **Proof of Proposition 3.** The first-order cross correlation $\Delta C_1^{(1)}$ is the sum of many terms, and we will study in detail one of them, the other terms can be addressed in the same way. These cross correlation terms involve one wave with one component $\hat{G}_1$ and another wave with only components of the form $\hat{G}_0$. This is a cross correlation of a wave that has been single-scattered by the medium with a wave that has not interacted with the medium. The term that we study is

$$\Delta C_{1,1}^{(1)}(\tau,\boldsymbol{x}_1,\boldsymbol{x}_2) = \frac{\sigma_{\rm r} l_{\rm r}^3}{2\pi c_0^2 \varepsilon^4} \iint \mathrm{d}\boldsymbol{y}\mathrm{d}\omega K(\boldsymbol{y})\omega^2 \hat{F}(\omega) \times \overline{\hat{G}_0}\Big(\frac{\omega}{\varepsilon},\boldsymbol{x}_1,\boldsymbol{z}_{\rm r}\Big)\overline{\hat{G}_0}\Big(\frac{\omega}{\varepsilon},\boldsymbol{z}_{\rm r},\boldsymbol{y}\Big)\,\hat{G}_1\Big(\frac{\omega}{\varepsilon},\boldsymbol{x}_2,\boldsymbol{y}\Big)e^{-i\frac{\omega}{\varepsilon}\tau},$$

which can also be written as

$$\Delta C_{1,1}^{(1)}(\tau,\boldsymbol{x}_1,\boldsymbol{x}_2) = \frac{\sigma_{\rm r} l_{\rm r}^3}{2\pi c_0^4 \varepsilon^4} \iiint \mathrm{d}\boldsymbol{y}\mathrm{d}\boldsymbol{z}\mathrm{d}\omega K(\boldsymbol{y})\omega^4 \hat{F}(\omega) \times \overline{\hat{G}_0}\Big(\frac{\omega}{\varepsilon},\boldsymbol{x}_1,\boldsymbol{z}_{\rm r}\Big)\overline{\hat{G}_0}\Big(\frac{\omega}{\varepsilon},\boldsymbol{z}_{\rm r},\boldsymbol{y}\Big)\,\hat{G}_0\Big(\frac{\omega}{\varepsilon},\boldsymbol{x}_2,\boldsymbol{z}\Big)V(\boldsymbol{z})\hat{G}_0\Big(\frac{\omega}{\varepsilon},\boldsymbol{z},\boldsymbol{y}\Big)e^{-i\frac{\omega}{\varepsilon}\tau}.$$

It is the cross correlation of a wave emitted by a source point at $\boldsymbol{y}$, reflected at $\boldsymbol{z}_{\rm r}$, and recorded at $\boldsymbol{x}_1$, with a wave emitted by the source point at $\boldsymbol{y}$, scattered at $\boldsymbol{z}$, and recorded at $\boldsymbol{x}_2$. Since $V(\boldsymbol{z})$ has mean zero, $\Delta C^{(1)}_{1,1}(\tau,\boldsymbol{x}_1,\boldsymbol{x}_2)$ has also mean zero. Using the delta-correlation property of V, we find that its variance is

$$\begin{aligned}\mathrm{Var}\big(\Delta C^{(1)}_{1,1}(\tau,\boldsymbol{x}_1,\boldsymbol{x}_2)\big) &= \frac{\sigma_{\rm r}^2 l_{\rm r}^6 \sigma_{\rm s}^2 l_{\rm s}^3}{4\pi^2 c_0^8 \varepsilon^8}\iiint \mathrm{d}\boldsymbol{y}_1\mathrm{d}\omega_1\mathrm{d}\boldsymbol{y}_2\mathrm{d}\omega_2\mathrm{d}\boldsymbol{z}\rho(\boldsymbol{z})\omega_1^4\hat F(\omega_1)\omega_2^4\hat F(\omega_2)\\ &\times K(\boldsymbol{y}_1)K(\boldsymbol{y}_2)\overline{\hat G_0}\Big(\frac{\omega_1}{\varepsilon},\boldsymbol{x}_1,\boldsymbol{z}_{\rm r}\Big)\overline{\hat G_0}\Big(\frac{\omega_1}{\varepsilon},\boldsymbol{z}_{\rm r},\boldsymbol{y}_1\Big)\overline{\hat G_0}\Big(\frac{\omega_2}{\varepsilon},\boldsymbol{x}_2,\boldsymbol{z}\Big)\overline{\hat G_0}\Big(\frac{\omega_2}{\varepsilon},\boldsymbol{z},\boldsymbol{y}_2\Big)\\ &\times\hat G_0\Big(\frac{\omega_1}{\varepsilon},\boldsymbol{x}_2,\boldsymbol{z}\Big)\hat G_0\Big(\frac{\omega_1}{\varepsilon},\boldsymbol{z},\boldsymbol{y}_1\Big)\hat G_0\Big(\frac{\omega_2}{\varepsilon},\boldsymbol{x}_1,\boldsymbol{z}_{\rm r}\Big)\hat G_0\Big(\frac{\omega_2}{\varepsilon},\boldsymbol{z}_{\rm r},\boldsymbol{y}_2\Big)e^{-i\frac{\omega_1-\omega_2}{\varepsilon}\tau},\end{aligned}$$

which can also be written as

$$\begin{aligned}\mathrm{Var}\big(\Delta C^{(1)}_{1,1}(\tau,\boldsymbol{x}_1,\boldsymbol{x}_2)\big) &= \frac{\sigma_{\rm r}^2 l_{\rm r}^6 \sigma_{\rm s}^2 l_{\rm s}^3}{2^{18}\pi^{10} c_0^8 \varepsilon^8}\iiint \mathrm{d}\boldsymbol{y}_1\mathrm{d}\omega_1\mathrm{d}\boldsymbol{y}_2\mathrm{d}\omega_2\mathrm{d}\boldsymbol{z}\rho(\boldsymbol{z})\\ &\times\frac{\omega_1^4\hat F(\omega_1)\omega_2^4\hat F(\omega_2)K(\boldsymbol{y}_1)K(\boldsymbol{y}_2)}{|\boldsymbol{x}_1-\boldsymbol{z}_{\rm r}|^2|\boldsymbol{x}_2-\boldsymbol{z}|^2|\boldsymbol{z}_{\rm r}-\boldsymbol{y}_1||\boldsymbol{z}-\boldsymbol{y}_2||\boldsymbol{z}-\boldsymbol{y}_1||\boldsymbol{z}_{\rm r}-\boldsymbol{y}_2|}e^{i\frac{\omega_1}{\varepsilon}\mathcal{T}_0(\boldsymbol{y}_1,\boldsymbol{z})}e^{-i\frac{\omega_2}{\varepsilon}\mathcal{T}_0(\boldsymbol{y}_2,\boldsymbol{z})},\end{aligned}$$

with

$$\mathcal{T}_0(\boldsymbol{y},\boldsymbol{z}) = -\mathcal{T}(\boldsymbol{x}_1,\boldsymbol{z}_{\rm r}) - \mathcal{T}(\boldsymbol{z}_{\rm r},\boldsymbol{y}) + \mathcal{T}(\boldsymbol{x}_2,\boldsymbol{z}) + \mathcal{T}(\boldsymbol{z},\boldsymbol{y}) - \tau.$$

Motivated by a stationary phase argument, we make the change of variables $(\omega_1,\omega_2) \mapsto (\omega,h) := (\frac{\omega_1+\omega_2}{2},\frac{\omega_1-\omega_2}{\varepsilon})$, which gives

$$\begin{aligned}\mathrm{Var}\big(\Delta C^{(1)}_{1,1}(\tau,\boldsymbol{x}_1,\boldsymbol{x}_2)\big) &= \frac{\sigma_{\rm r}^2 l_{\rm r}^6 \sigma_{\rm s}^2 l_{\rm s}^3}{2^{18}\pi^{10} c_0^8 \varepsilon^7}\iiint \mathrm{d}\boldsymbol{y}_1\mathrm{d}\boldsymbol{y}_2\mathrm{d}\omega\mathrm{d}h\mathrm{d}\boldsymbol{z}\rho(\boldsymbol{z})\\ &\times\frac{K(\boldsymbol{y}_1)K(\boldsymbol{y}_2)\omega^8\hat F^2(\omega)}{|\boldsymbol{x}_1-\boldsymbol{z}_{\rm r}|^2|\boldsymbol{x}_2-\boldsymbol{z}|^2|\boldsymbol{z}_{\rm r}-\boldsymbol{y}_1||\boldsymbol{z}-\boldsymbol{y}_2||\boldsymbol{z}-\boldsymbol{y}_1||\boldsymbol{z}_{\rm r}-\boldsymbol{y}_2|}e^{ih\mathcal{T}_s(\boldsymbol{y}_1,\boldsymbol{y}_2,\boldsymbol{z})}e^{i\frac{\omega}{\varepsilon}\mathcal{T}_r(\boldsymbol{y}_1,\boldsymbol{y}_2,\boldsymbol{z})},\end{aligned}$$

where the rapid and slow phases are given by

$$\begin{aligned}\mathcal{T}_r(\boldsymbol{y}_1,\boldsymbol{y}_2,\boldsymbol{z}) &= -\mathcal{T}(\boldsymbol{z}_{\rm r},\boldsymbol{y}_1) + \mathcal{T}(\boldsymbol{z}_{\rm r},\boldsymbol{y}_2) + \mathcal{T}(\boldsymbol{z},\boldsymbol{y}_1) - \mathcal{T}(\boldsymbol{z},\boldsymbol{y}_2),\\ \mathcal{T}_s(\boldsymbol{y}_1,\boldsymbol{y}_2,\boldsymbol{z}) &= -\mathcal{T}(\boldsymbol{x}_1,\boldsymbol{z}_{\rm r}) + \mathcal{T}(\boldsymbol{x}_2,\boldsymbol{z})\\ &\quad+\frac{1}{2}\big(-\mathcal{T}(\boldsymbol{z}_{\rm r},\boldsymbol{y}_1) - \mathcal{T}(\boldsymbol{z}_{\rm r},\boldsymbol{y}_2) + \mathcal{T}(\boldsymbol{z},\boldsymbol{y}_1) + \mathcal{T}(\boldsymbol{z},\boldsymbol{y}_2)\big) - \tau.\end{aligned}$$

In order to identify the dominant contribution we apply the stationary phase method. The stationary points should satisfy the four conditions

$$\partial_\omega\big(\omega\mathcal{T}_r\big) = 0, \quad \nabla_{\boldsymbol{y}_1}\big(\omega\mathcal{T}_r\big) = \boldsymbol{0}, \quad \nabla_{\boldsymbol{y}_2}\big(\omega\mathcal{T}_r\big) = \boldsymbol{0}, \quad \nabla_{\boldsymbol{z}}\big(\omega\mathcal{T}_r\big) = \boldsymbol{0}.$$

In the backlight illumination configuration this means that the four points should be along the same ray with $\boldsymbol{y}_1,\boldsymbol{y}_2 \to \boldsymbol{z}_{\rm r} \to \boldsymbol{z}$ or $\boldsymbol{y}_1,\boldsymbol{y}_2 \to \boldsymbol{z} \to \boldsymbol{z}_{\rm r}$.

We first study the contribution (i) of the scatterers $\boldsymbol{z}$ such that $\boldsymbol{y}_1,\boldsymbol{y}_2 \to \boldsymbol{z}_{\rm r} \to \boldsymbol{z}$. We introduce the unit vector

$$\hat{\boldsymbol{e}}_1 = \frac{\boldsymbol{z}_{\rm r}-\boldsymbol{z}}{|\boldsymbol{z}_{\rm r}-\boldsymbol{z}|}$$

and complete it with two other unit vectors $(\hat{\boldsymbol{e}}_2,\hat{\boldsymbol{e}}_3)$ so that $(\hat{\boldsymbol{e}}_1,\hat{\boldsymbol{e}}_2,\hat{\boldsymbol{e}}_3)$ is an orthonormal basis. We make the change of variables $\boldsymbol{y}_j \mapsto (a_j,b_j,c_j)$, for $j=1,2$:

$$\boldsymbol{y}_j = \boldsymbol{z}_{\rm r} + |\boldsymbol{z}_{\rm r}-\boldsymbol{z}|\big[a_j\hat{\boldsymbol{e}}_1 + \varepsilon^{1/2}b_j\hat{\boldsymbol{e}}_2 + \varepsilon^{1/2}c_j\hat{\boldsymbol{e}}_3\big],$$

with $a_j > 0$ since we consider here that $\boldsymbol{y}_j \to \boldsymbol{z}_{\rm r} \to \boldsymbol{z}$. The Jacobian of the change of variables is $\varepsilon|\boldsymbol{z}_{\rm r}-\boldsymbol{z}|^3$. This gives a parameterization of the variable $\boldsymbol{y}_j$ along the

ray joining $\boldsymbol{z}$ and $\boldsymbol{z}_{\rm r}$. We obtain

$$\mathrm{Var}\big(\Delta C^{(1)}_{1,1}(\tau,\boldsymbol{x}_1,\boldsymbol{x}_2)\big)^{(i)} = \frac{\sigma_{\rm r}^2 l_{\rm r}^6 \sigma_{\rm s}^2 l_{\rm s}^3}{2^{18}\pi^{10} c_0^8 \varepsilon^5} \iiint \mathrm{d}a_1 \mathrm{d}a_2 \mathrm{d}\omega \mathrm{d}h \mathrm{d}\boldsymbol{z} \rho(\boldsymbol{z}) |\boldsymbol{z}_{\rm r}-\boldsymbol{z}|^2$$
$$\times \frac{K(\boldsymbol{z}_{\rm r}+(\boldsymbol{z}_{\rm r}-\boldsymbol{z})a_1) K(\boldsymbol{z}_{\rm r}+(\boldsymbol{z}_{\rm r}-\boldsymbol{z})a_2) \omega^8 \hat F^2(\omega)}{|\boldsymbol{x}_1-\boldsymbol{z}_{\rm r}|^2 |\boldsymbol{x}_2-\boldsymbol{z}|^2 a_1(1+a_1)a_2(1+a_2)} e^{ih\mathcal{T}_s(\boldsymbol{z}_{\rm r}+(\boldsymbol{z}_{\rm r}-\boldsymbol{z})a_1, \boldsymbol{z}_{\rm r}+(\boldsymbol{z}_{\rm r}-\boldsymbol{z})a_2, \boldsymbol{z})}$$
$$\times \iint \mathrm{d}b_1 \mathrm{d}c_1 \mathrm{d}b_2 \mathrm{d}c_2 e^{-i\frac{\omega}{2c_0}\frac{b_1^2+c_1^2}{a_1(1+a_1)}|\boldsymbol{z}_{\rm r}-\boldsymbol{z}| + i\frac{\omega}{2c_0}\frac{b_2^2+c_2^2}{a_2(1+a_2)}|\boldsymbol{z}_{\rm r}-\boldsymbol{z}|}.$$

We compute the integrals in h, b_1, c_1, b_2, c_2 by making use of the identity

$$\int \mathrm{d}b e^{-i\frac{b^2}{2}} = \sqrt{2\pi} e^{-i\frac{\pi}{4}},$$

and we make the changes of variables $a_j = l_j/|\boldsymbol{z}_{\rm r}-\boldsymbol{z}|$, $j=1,2$, so that we obtain

$$\mathrm{Var}\big(\Delta C^{(1)}_{1,1}(\tau,\boldsymbol{x}_1,\boldsymbol{x}_2)\big)^{(i)} = \frac{\sigma_{\rm r}^2 l_{\rm r}^6 \sigma_{\rm s}^2 l_{\rm s}^3}{2^{15}\pi^7 c_0^5 \varepsilon^5} \iiint \mathrm{d}l_1 \mathrm{d}l_2 \mathrm{d}\omega \mathrm{d}\boldsymbol{z} \omega^6 \hat F^2(\omega) \rho(\boldsymbol{z})$$
$$\times \frac{K(\boldsymbol{z}_{\rm r}+\frac{\boldsymbol{z}_{\rm r}-\boldsymbol{z}}{|\boldsymbol{z}_{\rm r}-\boldsymbol{z}|}l_1) K(\boldsymbol{z}_{\rm r}+\frac{\boldsymbol{z}_{\rm r}-\boldsymbol{z}}{|\boldsymbol{z}_{\rm r}-\boldsymbol{z}|}l_2)}{|\boldsymbol{x}_1-\boldsymbol{z}_{\rm r}|^2 |\boldsymbol{x}_2-\boldsymbol{z}|^2 |\boldsymbol{z}_{\rm r}-\boldsymbol{z}|^2} \delta\big(|\boldsymbol{x}_2-\boldsymbol{z}| - |\boldsymbol{x}_1-\boldsymbol{z}_{\rm r}| + |\boldsymbol{z}_{\rm r}-\boldsymbol{z}| - c_0\tau\big),$$

which gives

$$\mathrm{Var}\big(\Delta C^{(1)}_{1,1}(\tau,\boldsymbol{x}_1,\boldsymbol{x}_2)\big)^{(i)} = \frac{\sigma_{\rm r}^2 l_{\rm r}^6 \sigma_{\rm s}^2 l_{\rm s}^3}{2^{15}\pi^7 c_0^5 \varepsilon^5} \Big[\int \mathrm{d}\omega \omega^6 \hat F^2(\omega)\Big]$$
$$\times \int \mathrm{d}\boldsymbol{z} \frac{K^2_{\boldsymbol{z}_{\rm r},\boldsymbol{z}} \rho(\boldsymbol{z})}{|\boldsymbol{x}_1-\boldsymbol{z}_{\rm r}|^2 |\boldsymbol{x}_2-\boldsymbol{z}|^2 |\boldsymbol{z}_{\rm r}-\boldsymbol{z}|^2}$$
$$\times \delta\big(|\boldsymbol{x}_2-\boldsymbol{z}| - |\boldsymbol{x}_1-\boldsymbol{z}_{\rm r}| + |\boldsymbol{z}_{\rm r}-\boldsymbol{z}| - c_0\tau\big).$$

We second study the contribution (ii) of the scatterers $\boldsymbol{z}$ such that $\boldsymbol{y}_1, \boldsymbol{y}_2 \to \boldsymbol{z} \to \boldsymbol{z}_{\rm r}$. We introduce the unit vector

$$\hat{\boldsymbol{e}}_1 = \frac{\boldsymbol{z}-\boldsymbol{z}_{\rm r}}{|\boldsymbol{z}-\boldsymbol{z}_{\rm r}|},$$

and we complete it with two other unit vectors $(\hat{\boldsymbol{e}}_2, \hat{\boldsymbol{e}}_3)$ so that $(\hat{\boldsymbol{e}}_1, \hat{\boldsymbol{e}}_2, \hat{\boldsymbol{e}}_3)$ is an orthonormal basis. We proceed as above and find

$$\mathrm{Var}\big(\Delta C^{(1)}_{1,1}(\tau,\boldsymbol{x}_1,\boldsymbol{x}_2)\big)^{(ii)} = \frac{\sigma_{\rm r}^2 l_{\rm r}^6 \sigma_{\rm s}^2 l_{\rm s}^3}{2^{15}\pi^7 c_0^5 \varepsilon^5} \Big[\int \mathrm{d}\omega \omega^6 \hat F^2(\omega)\Big]$$
$$\times \int \mathrm{d}\boldsymbol{z} \frac{K^2_{\boldsymbol{z},\boldsymbol{z}_{\rm r}} \rho(\boldsymbol{z})}{|\boldsymbol{x}_1-\boldsymbol{z}_{\rm r}|^2 |\boldsymbol{x}_2-\boldsymbol{z}|^2 |\boldsymbol{z}_{\rm r}-\boldsymbol{z}|^2}$$
$$\times \delta\big(|\boldsymbol{x}_2-\boldsymbol{z}| - |\boldsymbol{x}_1-\boldsymbol{z}_{\rm r}| - |\boldsymbol{z}_{\rm r}-\boldsymbol{z}| - c_0\tau\big).$$

The other terms can be addressed in the same way, and we find that the time-integrated variance has the form (45) while the variance for a fixed lag time τ is (42).

Appendix B. **Proof of Proposition 4.** The second-order cross correlation $\Delta C_2^{(1)}$ is the sum of many terms, which can be orgaized into two groups:
- We study in Subsection B.1 the first group, which contains the cross correlations of two waves that have been single-scattered by the medium. More exactly, the term that we study in detail in Subsection B.1 involves one component $\hat G_1$ for each of the two waves that are cross correlated.
- We study in Subsection B.2 the second group, which contains the cross correlations

of a wave that has been double-scattered by the medium with a wave that has not been scattered by the medium. More exactly, the term that we study in detail in Subsection B.2 involves two components $\hat{G}_1$ for one of the two waves that are cross correlated, while the other wave involves only $\hat{G}_0$. We also briefly address a term that involves one component $\hat{G}_2$ for one of the two waves that are cross correlated, while the other wave involves only $\hat{G}_0$, which is of the same form as the previous one.

B.1. **First group.** The first term that we address in detail is

$$\Delta C_{2,1}^{(1)}(\tau,\boldsymbol{x}_1,\boldsymbol{x}_2)=\frac{\sigma_{\rm r} l_{\rm r}^3}{2\pi c_0^2\varepsilon^6}\int \mathrm{d}\boldsymbol{y}\mathrm{d}\omega K(\boldsymbol{y})\omega^2\hat{F}(\omega)$$
$$\times\overline{\hat{G}_0}\Big(\frac{\omega}{\varepsilon},\boldsymbol{x}_1,\boldsymbol{z}_{\rm r}\Big)\overline{\hat{G}_1}\Big(\frac{\omega}{\varepsilon},\boldsymbol{z}_{\rm r},\boldsymbol{y}\Big)\,\hat{G}_1\Big(\frac{\omega}{\varepsilon},\boldsymbol{x}_2,\boldsymbol{y}\Big)e^{-i\frac{\omega}{\varepsilon}\tau},$$

which can also be written as

$$\Delta C_{2,1}^{(1)}(\tau,\boldsymbol{x}_1,\boldsymbol{x}_2)=\frac{\sigma_{\rm r} l_{\rm r}^3}{2\pi c_0^6\varepsilon^6}\iiint \mathrm{d}\boldsymbol{y}\mathrm{d}\boldsymbol{z}\mathrm{d}\boldsymbol{z}'\mathrm{d}\omega K(\boldsymbol{y})\omega^6\hat{F}(\omega)$$
$$\times\overline{\hat{G}_0}\Big(\frac{\omega}{\varepsilon},\boldsymbol{x}_1,\boldsymbol{z}_{\rm r}\Big)\overline{\hat{G}_0}\Big(\frac{\omega}{\varepsilon},\boldsymbol{z}_{\rm r},\boldsymbol{z}\Big)V(\boldsymbol{z})$$
$$\times\overline{\hat{G}_0}\Big(\frac{\omega}{\varepsilon},\boldsymbol{z},\boldsymbol{y}\Big)\,\hat{G}_0\Big(\frac{\omega}{\varepsilon},\boldsymbol{x}_2,\boldsymbol{z}'\Big)V(\boldsymbol{z}')\hat{G}_0\Big(\frac{\omega}{\varepsilon},\boldsymbol{z}',\boldsymbol{y}\Big)e^{-i\frac{\omega}{\varepsilon}\tau}.$$

It is the cross correlation of a wave emitted by a source point at $\boldsymbol{y}$, scattered at $\boldsymbol{z}$, reflected at $\boldsymbol{z}_{\rm r}$, and recorded at $\boldsymbol{x}_1$, with a wave emitted by the source point at $\boldsymbol{y}$, scattered at $\boldsymbol{z}'$, and recorded at $\boldsymbol{x}_2$. Using the delta-correlation property of V, its mean is

$$\mathbb{E}[\Delta C_{2,1}^{(1)}(\tau,\boldsymbol{x}_1,\boldsymbol{x}_2)]=\frac{\sigma_{\rm r} l_{\rm r}^3\sigma_{\rm s}^2 l_{\rm s}^3}{2\pi c_0^6\varepsilon^6}\iiint \mathrm{d}\boldsymbol{y}\mathrm{d}\boldsymbol{z}\mathrm{d}\omega K(\boldsymbol{y})\rho(\boldsymbol{z})\omega^6\hat{F}(\omega)$$
$$\times\overline{\hat{G}_0}\Big(\frac{\omega}{\varepsilon},\boldsymbol{x}_1,\boldsymbol{z}_{\rm r}\Big)\overline{\hat{G}_0}\Big(\frac{\omega}{\varepsilon},\boldsymbol{z}_{\rm r},\boldsymbol{z}\Big)\overline{\hat{G}_0}\Big(\frac{\omega}{\varepsilon},\boldsymbol{z},\boldsymbol{y}\Big)\,\hat{G}_0\Big(\frac{\omega}{\varepsilon},\boldsymbol{x}_2,\boldsymbol{z}\Big)\hat{G}_0\Big(\frac{\omega}{\varepsilon},\boldsymbol{z},\boldsymbol{y}\Big)e^{-i\frac{\omega}{\varepsilon}\tau},$$

which can also be written as

$$\mathbb{E}[\Delta C_{2,1}^{(1)}(\tau,\boldsymbol{x}_1,\boldsymbol{x}_2)]=\frac{\sigma_{\rm r} l_{\rm r}^3\sigma_{\rm s}^2 l_{\rm s}^3}{2^{11}\pi^6 c_0^6\varepsilon^6}\iiint \mathrm{d}\boldsymbol{y}\mathrm{d}\boldsymbol{z}\mathrm{d}\omega K(\boldsymbol{y})\rho(\boldsymbol{z})\omega^6\hat{F}(\omega)$$
$$\times\frac{1}{|\boldsymbol{x}_1-\boldsymbol{z}_{\rm r}||\boldsymbol{z}_{\rm r}-\boldsymbol{z}||\boldsymbol{z}-\boldsymbol{y}|^2|\boldsymbol{x}_2-\boldsymbol{z}|}e^{i\frac{\omega}{\varepsilon}\mathcal{T}_0(\boldsymbol{y},\boldsymbol{z})},$$

where the rapid phase is

$$\mathcal{T}_0(\boldsymbol{y},\boldsymbol{z})=-\mathcal{T}(\boldsymbol{x}_1,\boldsymbol{z}_{\rm r})-\mathcal{T}(\boldsymbol{z}_{\rm r},\boldsymbol{z})+\mathcal{T}(\boldsymbol{x}_2,\boldsymbol{z})-\tau.$$

This is the cross correlation of waves that have interacted once with the scattering medium and once with the reflector with waves that have interacted once with the scattering medium. That is why the average (with respect to the scattering medium) is not zero.

The stationary points satisfy the three conditions

$$\partial_\omega\big(\omega\mathcal{T}_0\big)=0,\quad \nabla_{\boldsymbol{y}}\big(\omega\mathcal{T}_0\big)=\boldsymbol{0},\quad \nabla_{\boldsymbol{z}}\big(\omega\mathcal{T}_0\big)=\boldsymbol{0}.$$

The rapid phase does not depend on $\boldsymbol{y}$, so the stationary points need to fulfill the two conditions

$$\nabla_{\boldsymbol{z}}\mathcal{T}(\boldsymbol{z},\boldsymbol{x}_2)=\nabla_{\boldsymbol{z}}\mathcal{T}(\boldsymbol{z},\boldsymbol{z}_{\rm r})\text{ and }\mathcal{T}(\boldsymbol{x}_2,\boldsymbol{z})-\mathcal{T}(\boldsymbol{x}_1,\boldsymbol{z}_{\rm r})-\mathcal{T}(\boldsymbol{z}_{\rm r},\boldsymbol{z})=\tau.$$

The first condition means that $\boldsymbol{x}_2$ and $\boldsymbol{z}_{\rm r}$ must be on the same ray issued from $\boldsymbol{z}$.

If $\boldsymbol{z} \to \boldsymbol{z}_{\rm r} \to \boldsymbol{x}_2$, then the second condition means $\tau = -\mathcal{T}(\boldsymbol{x}_1, \boldsymbol{z}_{\rm r}) + \mathcal{T}(\boldsymbol{x}_2, \boldsymbol{z}_{\rm r})$. This corresponds to a backlight illumination from the secondary source $\boldsymbol{z}$.

If $\boldsymbol{z} \to \boldsymbol{x}_2 \to \boldsymbol{z}_{\rm r}$, then the second condition means $\tau = -\mathcal{T}(\boldsymbol{x}_1, \boldsymbol{z}_{\rm r}) - \mathcal{T}(\boldsymbol{x}_2, \boldsymbol{z}_{\rm r})$. This is the contribution corresponding to a daylight illumination from the secondary source $\boldsymbol{z}$ and shown in the right Figure 6. We focus our attention to the backlight illumination configuration. We introduce the unit vector

$$\hat{\boldsymbol{e}}_1 = \frac{\boldsymbol{x}_2 - \boldsymbol{z}_{\rm r}}{|\boldsymbol{x}_2 - \boldsymbol{z}_{\rm r}|},$$

and we complete it with two other unit vectors $(\hat{\boldsymbol{e}}_2, \hat{\boldsymbol{e}}_3)$ so that $(\hat{\boldsymbol{e}}_1, \hat{\boldsymbol{e}}_2, \hat{\boldsymbol{e}}_3)$ is an orthonormal basis. We make the change of variables $\boldsymbol{z} \mapsto (a, b, c)$ with

$$\boldsymbol{z} = \boldsymbol{x}_2 + |\boldsymbol{x}_2 - \boldsymbol{z}_{\rm r}|\big[a\hat{\boldsymbol{e}}_1 + \varepsilon^{1/2} b\hat{\boldsymbol{e}}_2 + \varepsilon^{1/2} c\hat{\boldsymbol{e}}_3\big].$$

This gives a parameterization of the variable $\boldsymbol{z}$ along the ray joining $\boldsymbol{x}_2$ and $\boldsymbol{z}_{\rm r}$. Here the scatterers are behind the sensor array which means that we restrict ourselves to $a > 0$. We also parameterize the lag time τ around the difference of travel times:

$$\tau = -\mathcal{T}(\boldsymbol{x}_2, \boldsymbol{z}_{\rm r}) - \mathcal{T}(\boldsymbol{x}_1, \boldsymbol{z}_{\rm r}) + \varepsilon s.$$

We perform a Taylor series expansion of the rapid phase

$$\begin{aligned}
&\mathbb{E}[\Delta C_{2,1}^{(1)}(\tau, \boldsymbol{x}_1, \boldsymbol{x}_2)] \\
&= \frac{\sigma_{\rm r} l_{\rm r}^3 \sigma_{\rm s}^2 l_{\rm s}^2 |\boldsymbol{x}_2 - \boldsymbol{z}_{\rm r}|}{2^{11}\pi^6 c_0^6 \varepsilon^5 |\boldsymbol{x}_1 - \boldsymbol{z}_{\rm r}|} \iiint {\rm d}a{\rm d}\boldsymbol{y}{\rm d}\omega \omega^6 \hat{F}(\omega) \frac{K(\boldsymbol{y})\rho(\boldsymbol{x}_2 + a(\boldsymbol{x}_2 - \boldsymbol{z}_{\rm r}))}{a(1+a)} \\
&\quad \times \frac{1}{|\boldsymbol{x}_2 + a(\boldsymbol{x}_2 - \boldsymbol{z}_{\rm r}) - \boldsymbol{y}|^2} e^{-i\omega s} \iint {\rm d}b{\rm d}c e^{i\frac{\omega}{2c_0}\frac{b^2+c^2}{a(1+a)}|\boldsymbol{x}_2 - \boldsymbol{z}_{\rm r}|} \\
&= \frac{\sigma_{\rm r} l_{\rm r}^3 \sigma_{\rm s}^2 l_{\rm s}^2}{2^{10}\pi^5 c_0^5 \varepsilon^5 |\boldsymbol{x}_1 - \boldsymbol{z}_{\rm r}||\boldsymbol{x}_2 - \boldsymbol{z}_{\rm r}|} \\
&\quad \times \Big[\int {\rm d}\omega (i\omega^5) \hat{F}(\omega) e^{-i\omega s}\Big] \iiint {\rm d}a{\rm d}\boldsymbol{y} \frac{K(\boldsymbol{y})\rho(\boldsymbol{x}_2 + a(\boldsymbol{x}_2 - \boldsymbol{z}_{\rm r}))}{|\boldsymbol{x}_2 + a(\boldsymbol{x}_2 - \boldsymbol{z}_{\rm r}) - \boldsymbol{y}|^2} \\
&= -\frac{\sigma_{\rm r} l_{\rm r}^3 \sigma_{\rm s}^2 l_{\rm s}^2}{2^9\pi^4 c_0^5 \varepsilon^5 |\boldsymbol{x}_1 - \boldsymbol{z}_{\rm r}||\boldsymbol{x}_2 - \boldsymbol{z}_{\rm r}|} \Big[\int {\rm d}l K^\rho\Big(\boldsymbol{x}_2 + l\frac{\boldsymbol{x}_2 - \boldsymbol{z}_{\rm r}}{|\boldsymbol{x}_2 - \boldsymbol{z}_{\rm r}|}\Big)\Big] \partial_{\rm s}^5 F(s),
\end{aligned}$$

where K^ρ is defined by (48).

The analysis of the other terms involving one single-scattering component $\hat{G}_1$ for each of the two waves that are cross-correlated is similar.

B.2. **Second group.** The cross correlation terms that involve one wave with two components $\hat{G}_1$ and one wave with only $\hat{G}_0$ are dealt with according to the following way. These terms involve double-scattering events with respect to the randomly scattering medium, but they have to be taken into account because they are a priori of the same order of magnitude as the terms studied above, which involve the cross correlation of two waves with one single scattering event for each. One of these terms is

$$\begin{aligned}
\Delta C_{2,2}^{(1)}(\tau, \boldsymbol{x}_1, \boldsymbol{x}_2) = \frac{\sigma_{\rm r} l_{\rm r}^3}{2\pi c_0^2 \varepsilon^6} \int {\rm d}\boldsymbol{y}{\rm d}\omega K(\boldsymbol{y}) \omega^2 \hat{F}(\omega) \\
\times \overline{\hat{G}_1}\Big(\frac{\omega}{\varepsilon}, \boldsymbol{x}_1, \boldsymbol{z}_{\rm r}\Big) \overline{\hat{G}_1}\Big(\frac{\omega}{\varepsilon}, \boldsymbol{z}_{\rm r}, \boldsymbol{y}\Big) \hat{G}_0\Big(\frac{\omega}{\varepsilon}, \boldsymbol{x}_2, \boldsymbol{y}\Big) e^{-i\frac{\omega}{\varepsilon}\tau},
\end{aligned}$$

which can also be written as

$$\Delta C^{(1)}_{2,2}(\tau,\boldsymbol{x}_1,\boldsymbol{x}_2)=\frac{\sigma_{\rm r} l_{\rm r}^3}{2\pi c_0^6\varepsilon^6}\iiint \mathrm{d}\boldsymbol{y}\mathrm{d}\boldsymbol{z}\mathrm{d}\boldsymbol{z}'\mathrm{d}\omega K(\boldsymbol{y})\omega^6\hat{F}(\omega)$$
$$\times\overline{\hat{G}_0}\Big(\frac{\omega}{\varepsilon},\boldsymbol{x}_1,\boldsymbol{z}'\Big)V(\boldsymbol{z}')\overline{\hat{G}_0}\Big(\frac{\omega}{\varepsilon},\boldsymbol{z}',\boldsymbol{z}_{\rm r}\Big)$$
$$\times\overline{\hat{G}_0}\Big(\frac{\omega}{\varepsilon},\boldsymbol{z}_{\rm r},\boldsymbol{z}\Big)V(\boldsymbol{z})\overline{\hat{G}_0}\Big(\frac{\omega}{\varepsilon},\boldsymbol{z},\boldsymbol{y}\Big)\,\hat{G}_0\Big(\frac{\omega}{\varepsilon},\boldsymbol{x}_2,\boldsymbol{y}\Big)e^{-i\frac{\omega}{\varepsilon}\tau}.$$

The term $\Delta C^{(1)}_{2,2}$ is the cross correlation of a wave emitted by a source point at $\boldsymbol{y}$, scattered at $\boldsymbol{z}$, reflected at $\boldsymbol{z}_{\rm r}$, scattered at $\boldsymbol{z}'$, and recorded at $\boldsymbol{x}_1$, with a wave emitted by the source point at $\boldsymbol{y}$ and recorded at $\boldsymbol{x}_2$. Its mean is

$$\mathbb{E}[\Delta C^{(1)}_{2,2}(\tau,\boldsymbol{x}_1,\boldsymbol{x}_2)]=\frac{\sigma_{\rm r} l_{\rm r}^3\sigma_{\rm s}^2 l_{\rm s}^3}{2\pi c_0^6\varepsilon^6}\iiint \mathrm{d}\boldsymbol{y}\mathrm{d}\boldsymbol{z}\mathrm{d}\omega K(\boldsymbol{y})\rho(\boldsymbol{z})\omega^6\hat{F}(\omega)$$
$$\times\overline{\hat{G}_0}\Big(\frac{\omega}{\varepsilon},\boldsymbol{x}_1,\boldsymbol{z}\Big)\overline{\hat{G}_0}\Big(\frac{\omega}{\varepsilon},\boldsymbol{z}_{\rm r},\boldsymbol{z}\Big)^2\overline{\hat{G}_0}\Big(\frac{\omega}{\varepsilon},\boldsymbol{z},\boldsymbol{y}\Big)\,\hat{G}_0\Big(\frac{\omega}{\varepsilon},\boldsymbol{x}_2,\boldsymbol{y}\Big)e^{-i\frac{\omega}{\varepsilon}\tau},$$

which can also be written as

$$\mathbb{E}[\Delta C^{(1)}_{2,2}(\tau,\boldsymbol{x}_1,\boldsymbol{x}_2)]=\frac{\sigma_{\rm r} l_{\rm r}^3\sigma_{\rm s}^2 l_{\rm s}^3}{2^{11}\pi^6 c_0^6\varepsilon^6}\iiint \mathrm{d}\boldsymbol{y}\mathrm{d}\boldsymbol{z}\mathrm{d}\omega K(\boldsymbol{y})\rho(\boldsymbol{z})\omega^6\hat{F}(\omega)$$
$$\times\frac{1}{|\boldsymbol{x}_1-\boldsymbol{z}||\boldsymbol{z}-\boldsymbol{z}_{\rm r}|^2|\boldsymbol{z}-\boldsymbol{y}||\boldsymbol{x}_2-\boldsymbol{y}|}e^{i\frac{\omega}{\varepsilon}\mathcal{T}_0(\boldsymbol{y},\boldsymbol{z})},$$

where the rapid phase is

$$\mathcal{T}_0(\boldsymbol{y},\boldsymbol{z})=-\mathcal{T}(\boldsymbol{x}_1,\boldsymbol{z})-2\mathcal{T}(\boldsymbol{z}_{\rm r},\boldsymbol{z})-\mathcal{T}(\boldsymbol{z},\boldsymbol{y})+\mathcal{T}(\boldsymbol{x}_2,\boldsymbol{y})-\tau.$$

The stationary points satisfy the three conditions

$$\partial_\omega\big(\omega\mathcal{T}_0\big)=0,\quad \nabla_{\boldsymbol{y}}\big(\omega\mathcal{T}_0\big)=\boldsymbol{0},\quad \nabla_{\boldsymbol{z}}\big(\omega\mathcal{T}_0\big)=\boldsymbol{0},$$

that is to say:

$$\nabla_{\boldsymbol{y}}\mathcal{T}(\boldsymbol{y},\boldsymbol{x}_2)=\nabla_{\boldsymbol{y}}\mathcal{T}(\boldsymbol{y},\boldsymbol{z}),\quad \nabla_{\boldsymbol{z}}\mathcal{T}(\boldsymbol{z},\boldsymbol{x}_2)+2\nabla_{\boldsymbol{z}}\mathcal{T}(\boldsymbol{z},\boldsymbol{z}_{\rm r})+\nabla_{\boldsymbol{z}}\mathcal{T}(\boldsymbol{z},\boldsymbol{y})=\boldsymbol{0},$$

and

$$\mathcal{T}(\boldsymbol{x}_2,\boldsymbol{y})-\mathcal{T}(\boldsymbol{x}_1,\boldsymbol{z})-2\mathcal{T}(\boldsymbol{z}_{\rm r},\boldsymbol{z})-\mathcal{T}(\boldsymbol{z},\boldsymbol{y})=\tau.$$

The second condition (in $\nabla_{\boldsymbol{z}}$) cannot be fulfilled in our geometry (Figure 7a), in which the scatterers $\boldsymbol{z}$ are on the opposite side of the sensor $\boldsymbol{x}_2$, the reflector $\boldsymbol{z}_{\rm r}$, and the sources $\boldsymbol{y}$. Therefore the term $\mathbb{E}[\Delta C^{(1)}_{2,2}(\tau,\boldsymbol{x}_1,\boldsymbol{x}_2)]$ gives a negligible contribution.

The cross correlation terms that involve one wave with one component $\hat{G}_2$ and one wave with only $\hat{G}_0$ have similar properties as the term $\Delta C^{(1)}_{2,2}$ studied here above, in the sense that it is not possible to find stationary points or maps of points that give a contribution to their expectations. This is again due to our geometry in which the scatterers are on the opposite side of the sensor array, the reflector, and the sources. Therefore they do not contribute to the mean of the cross correlation.

Appendix C. **Proof of Proposition 5.** The proof of Proposition 5 is not completely obvious because the virtual sources are fully correlated with the noise sources. By expanding the expression of the cross correlation in terms of the background

Green's function $\hat{G}_0$, we obtain that the differential cross correlation is the contribution of sixteen terms, which correspond to take into account the virtual sources and the virtual reflector. We will study in detail one of them:

$$\Delta C_1^{(1)}(\tau,\boldsymbol{x}_1,\boldsymbol{x}_2)=\frac{\sigma_{\rm r} l_{\rm r}^3 R_{\rm m}^2}{2^7\pi^4 c_0^2\varepsilon^2}\iint {\rm d}\boldsymbol{y}{\rm d}\omega\omega^2\hat{F}(\omega)\frac{K(\boldsymbol{y})}{|\tilde{\boldsymbol{y}}-\boldsymbol{x}_1||\tilde{\boldsymbol{y}}-\boldsymbol{z}_{\rm r}||\boldsymbol{z}_{\rm r}-\boldsymbol{x}_2|}e^{i\frac{\omega}{\varepsilon}\mathcal{T}_0(\boldsymbol{y})},$$

where the rapid phase is

$$\mathcal{T}_0(\boldsymbol{y})=-\mathcal{T}(\tilde{\boldsymbol{y}},\boldsymbol{x}_1)+\mathcal{T}(\tilde{\boldsymbol{y}},\boldsymbol{z}_{\rm r})+\mathcal{T}(\boldsymbol{z}_{\rm r},\boldsymbol{x}_2)-\tau.$$

We use the fact that $\mathcal{T}(\boldsymbol{x},\tilde{\boldsymbol{y}})=\mathcal{T}(\tilde{\boldsymbol{x}},\boldsymbol{y})$ for any pair of points $(\boldsymbol{x},\boldsymbol{y})$ and we apply the stationary phase method. The dominant contribution comes from the stationary points that satisfy

$$\nabla_{\boldsymbol{y}}\big(\omega\mathcal{T}_0(\boldsymbol{y})\big)=\boldsymbol{0},\quad \partial_\omega\big(\omega\mathcal{T}_0(\boldsymbol{y})\big)=0,$$

which reads

$$\nabla_{\boldsymbol{y}}\mathcal{T}(\boldsymbol{y},\tilde{\boldsymbol{x}}_1)=\nabla_{\boldsymbol{y}}\mathcal{T}(\boldsymbol{y},\tilde{\boldsymbol{z}}_{\rm r}),\quad \tau=-\mathcal{T}(\tilde{\boldsymbol{y}},\boldsymbol{x}_1)+\mathcal{T}(\tilde{\boldsymbol{y}},\boldsymbol{z}_{\rm r})+\mathcal{T}(\boldsymbol{z}_{\rm r},\boldsymbol{x}_2).$$

The first condition imposes that $\tilde{\boldsymbol{x}}_1$ and $\tilde{\boldsymbol{z}}_{\rm r}$ are on the same ray issued from $\boldsymbol{y}$, which is equivalent to the condition that $\boldsymbol{x}_1$ and $\boldsymbol{z}_{\rm r}$ are on the same ray issued from $\tilde{\boldsymbol{y}}$. The second condition then reads

$$\tau=\pm\mathcal{T}(\boldsymbol{z}_{\rm r},\boldsymbol{x}_1)+\mathcal{T}(\boldsymbol{z}_{\rm r},\boldsymbol{x}_2),$$

with the sign + (resp. −) if $\boldsymbol{z}_{\rm r}\to\boldsymbol{x}_1\to\tilde{\boldsymbol{y}}$ (resp. $\boldsymbol{x}_1\to\boldsymbol{z}_{\rm r}\to\tilde{\boldsymbol{y}}$).

We focus our attention to the backlight illumination configuration $\boldsymbol{z}_{\rm r}\to\boldsymbol{x}_1\to\tilde{\boldsymbol{y}}$. Using the change of variable $\boldsymbol{y}\mapsto\tilde{\boldsymbol{y}}$, we find

$$\Delta C_1^{(1)}(\tau,\boldsymbol{x}_1,\boldsymbol{x}_2)=\frac{\sigma_{\rm r} l_{\rm r}^3 R_{\rm m}^2}{2^7\pi^4 c_0^2\varepsilon^2}\iint {\rm d}\boldsymbol{y}{\rm d}\omega\omega^2\hat{F}(\omega)\frac{\widetilde{K}(\boldsymbol{y})}{|\boldsymbol{y}-\boldsymbol{x}_1||\boldsymbol{y}-\boldsymbol{z}_{\rm r}||\boldsymbol{z}_{\rm r}-\boldsymbol{x}_2|}\times e^{i\frac{\omega}{\varepsilon}(-\mathcal{T}(\boldsymbol{y},\boldsymbol{x}_1)+\mathcal{T}(\boldsymbol{y},\boldsymbol{z}_{\rm r})+\mathcal{T}(\boldsymbol{z}_{\rm r},\boldsymbol{x}_2)-\tau)}.$$

The analysis using the stationary phase theorem then goes along the same lines as in the previous appendices. The analysis of the other terms is similar and completes the proof.

Appendix D. **Inter-sensor travel time estimation with coda cross correlations.** It is possible to estimate the travel time between two sensors $\boldsymbol{x}_1$ and $\boldsymbol{x}_2$ in a scattering medium by looking at the main peaks of a special fourth-order cross correlation $C_T^{(3)}(\tau,\boldsymbol{x}_1,\boldsymbol{x}_2)$. This fourth-order cross correlation uses the data recorded by an array of auxiliary sensors $\boldsymbol{x}_{{\rm a},k}$, $k=1,\ldots,N_{\rm a}$, and it is evaluated as follows.

1) Calculate the cross correlations between $\boldsymbol{x}_1$ and $\boldsymbol{x}_{{\rm a},k}$ and between $\boldsymbol{x}_2$ and $\boldsymbol{x}_{{\rm a},k}$ for each auxiliary sensor $\boldsymbol{x}_{{\rm a},k}$:

$$C_T(\tau,\boldsymbol{x}_{{\rm a},k},\boldsymbol{x}_l)=\frac{1}{T}\int_0^T u(t,\boldsymbol{x}_{{\rm a},k})u(t+\tau,\boldsymbol{x}_l){\rm d}t,\qquad l=1,2,\quad k=1,\ldots,N_a.$$

2) Calculate the coda (i.e. the tails) of these cross correlations:

$$C_{T,{\rm coda}}(\tau,\boldsymbol{x}_{{\rm a},k},\boldsymbol{x}_l)=C_T(\tau,\boldsymbol{x}_{{\rm a},k},\boldsymbol{x}_l)\mathbf{1}_{[T_{\rm c1},T_{\rm c2}]}(|\tau|),\qquad l=1,2,\quad k=1,\ldots,N_a.$$

3) Cross correlate the tails of the cross correlations and sum them over all auxiliary sensors to form the coda cross correlation between $\boldsymbol{x}_1$ and $\boldsymbol{x}_2$:

$$C_T^{(3)}(\tau,\boldsymbol{x}_1,\boldsymbol{x}_2)=\sum_{k=1}^{N_{\rm a}}\int C_{T,{\rm coda}}(\tau',\boldsymbol{x}_{{\rm a},k},\boldsymbol{x}_1)C_{T,{\rm coda}}(\tau'+\tau,\boldsymbol{x}_{{\rm a},k},\boldsymbol{x}_2){\rm d}\tau'.$$

The roles of the three parameters T, T_{c1}, and T_{c2} are described in Subsection 6.1. The coda cross correlation $C_T^{(3)}$ is a self-averaging quantity and it is equal to the statistical coda cross correlation $C^{(3)}$ as $T \to \infty$:

$$C^{(3)}(\tau, \boldsymbol{x}_1, \boldsymbol{x}_2) = \sum_{k=1}^{N_a} \int \overline{\hat{C}^{(1)}_{\text{coda}}}(\omega, \boldsymbol{x}_{a,k}, \boldsymbol{x}_1) \hat{C}^{(1)}_{\text{coda}}(\omega, \boldsymbol{x}_{a,k}, \boldsymbol{x}_2) e^{-i\omega\tau} d\omega,$$

$$C^{(1)}_{\text{coda}}(\tau, \boldsymbol{x}_{a,k}, \boldsymbol{x}_l) = C^{(1)}(\tau, \boldsymbol{x}_{a,k}, \boldsymbol{x}_l) \mathbf{1}_{[T_{c1}, T_{c2}]}(|\tau|).$$

The statistical coda cross correlation $C^{(3)}$ was studied in [13] by a stationary phase analysis. It differs from the statistical cross correlation $C^{(1)}$ in that the contributions of the direct waves are eliminated and only the contributions of the scattered waves are taken into account (note that some of the contributions of scattered waves are also eliminated, but only those which correspond to small additional travel times, which are also those which induce small directional diversity). Since scattered waves have more directional diversity than the direct waves when the noise sources are spatially localized, the coda cross correlation $C^{(3)}(\tau, \boldsymbol{x}_1, \boldsymbol{x}_2)$ usually exhibits a stronger peak at lag time equal to the inter-sensor travel time $\mathcal{T}(\boldsymbol{x}_1, \boldsymbol{x}_2)$. In particular, in contrast with the cross correlation $C^{(1)}$, the existence of a singular component at lag time equal to the travel time $\mathcal{T}(\boldsymbol{x}_1, \boldsymbol{x}_2)$ does not require that the ray joining $\boldsymbol{x}_1$ and $\boldsymbol{x}_2$ reaches into the source region, but only into the scattering region.

We illustrate these results in Figures 13-14 in which the five sensors are aligned perpendicularly to the energy flux coming from the noise sources and the cross correlation $C^{(1)}(\tau, \boldsymbol{x}_1, \boldsymbol{x}_j)$, $j = 1, \ldots, 5$ does not have a peak at lag time equal to the travel time between the sensors $\boldsymbol{x}_1$ and $\boldsymbol{x}_j$. In Figure 13 the ray going through the sensors $\boldsymbol{x}_1$ and $\boldsymbol{x}_j$ intersects the scattering layer and the coda cross correlation $C^{(3)}(\tau, \boldsymbol{x}_1, \boldsymbol{x}_j)$ has a peak at lag time equal to the travel time between the sensors. In Figure 14 the ray going through the sensors $\boldsymbol{x}_1$ and $\boldsymbol{x}_j$ does not intersect the scattering layer and the coda cross correlation $C^{(3)}(\tau, \boldsymbol{x}_1, \boldsymbol{x}_j)$ does not have a peak at lag time equal to the travel time between the sensors. Note the presence of the auxiliary sensors that are necessary for the evaluation of the coda cross correlation.

REFERENCES

[1] C. Bardos, J. Garnier and G. Papanicolaou, Identification of Green's functions singularities by cross correlation of noisy signals, *Inverse Problems*, **24** (2008), 015011, 26 pp.

[2] J. Berryman, Stable iterative reconstruction algorithm for nonlinear travel time tomography, *Inverse Problems*, **6** (1990), 21–42.

[3] B. L. Biondi, *3D Seismic Imaging*, no. 14 in Investigations in Geophysics, Society of Exploration Geophysics, Tulsa, 2006.

[4] N. Bleistein and R. Handelsman, *Asymptotic Expansions of Integrals*, Dover, New York, 1986.

[5] M. Born and E. Wolf, *Principles of Optics*, Cambridge University Press, Cambridge, 1999.

[6] F. Brenguier, N. M. Shapiro, M. Campillo, V. Ferrazzini, Z. Duputel, O. Coutant and A. Nercessian, Towards forecasting volcanic eruptions using seismic noise, *Nature Geoscience*, **1** (2008), 126–130.

[7] T. Callaghan, N. Czink, F. Mani, A. Paulraj and G. Papanicolaou, Correlation-based radio localization in an indoor environment, *EURASIP Journal on Wireless Communications and Networking*, **2011** (2011), 135p.

[8] J. F. Claerbout, *Imaging the Earth's Interior*, Blackwell Scientific Publications, Palo Alto, 1985.

[9] Y. Colin de Verdière, Semiclassical analysis and passive imaging, *Nonlinearity*, **22** (2009), R45–R75.

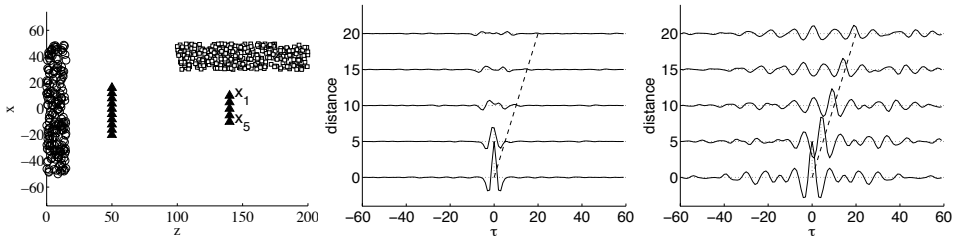

a) Configuration **b)** $C^{(1)}(\tau, \boldsymbol{x}_1, \boldsymbol{x}_j)$ **c)** $C^{(3)}(\tau, \boldsymbol{x}_1, \boldsymbol{x}_j)$

FIGURE 13. The configuration is shown in Figure a: the circles are the noise sources, the squares are the scatterers, and the triangles are the sensors. Figure b shows the cross correlation $C^{(1)}$ between the pairs of sensors $(\boldsymbol{x}_1, \boldsymbol{x}_j)$, $j = 1, \ldots, 5$, versus the distance $|\boldsymbol{x}_j - \boldsymbol{x}_1|$. Figure c shows the coda cross correlation $C^{(3)}$ between the pairs of sensors $(\boldsymbol{x}_1, \boldsymbol{x}_j)$, $j = 1, \ldots, 5$, which shows the singular peak at lag time equal to the travel time $\mathcal{T}(\boldsymbol{x}_1, \boldsymbol{x}_j)$ in the coda cross correlation $C^{(3)}$, because the ray going through $\boldsymbol{x}_1$ and $\boldsymbol{x}_j$ intersects the scattering region.

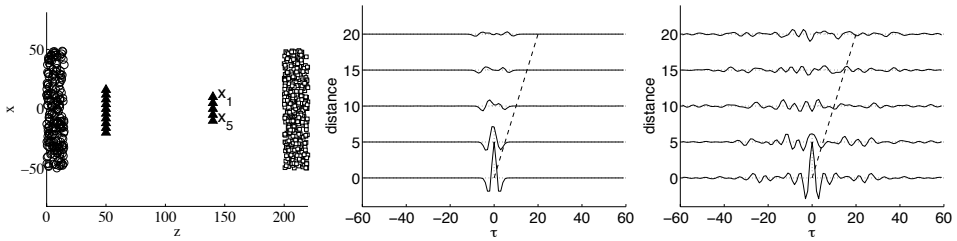

a) Configuration **b)** $C^{(1)}(\tau, \boldsymbol{x}_1, \boldsymbol{x}_j)$ **c)** $C^{(3)}(\tau, \boldsymbol{x}_1, \boldsymbol{x}_j)$

FIGURE 14. Same as in Figure 14 but here the scatterers are behind the sensor array and there is no singular peak at lag time equal to the travel time $\mathcal{T}(\boldsymbol{x}_1, \boldsymbol{x}_j)$ in the coda cross correlation $C^{(3)}$, because the ray going through $\boldsymbol{x}_1$ and $\boldsymbol{x}_j$ does not intersect the scattering region.

[10] L. Erdös and H.-T. Yau, Linear Boltzmann equation as the weak coupling limit of the random Schrödinger equation, *Comm. Pure Appl. Math.,* **53** (2000), 667–735.
[11] J.-P. Fouque, J. Garnier, G. Papanicolaou and K. Sølna, *Wave Propagation and Time Reversal in Randomly Layered Media*, Springer, New York, 2007.
[12] U. Frisch, Wave Propagation in Random Media, in *Probabilistic Methods in Applied Mathematics,* edited by A. T. Bharucha-Reid, Academic Press, New York, **1** (1968), 75–198.
[13] J. Garnier and G. Papanicolaou, Passive sensor imaging using cross correlations of noisy signals in a scattering medium, *SIAM J. Imaging Sciences,* **2** (2009), 396–437.
[14] J. Garnier and G. Papanicolaou, Resolution analysis for imaging with noise, *Inverse Problems*, **26** (2010), 074001, 22pp.
[15] J. Garnier and K. Sølna, Cross correlation and deconvolution of noise signals in randomly layered media, *SIAM J. Imaging Sciences,* **3** (2010), 809–834.
[16] O. A. Godin, Accuracy of the deterministic travel time retrieval from cross-correlations of non-diffuse ambient noise, *J. Acoust. Soc. Am.,* **126** (2009), EL183–EL189.

[17] P. Gouédard, L. Stehly, F. Brenguier, M. Campillo, Y. Colin de Verdière, E. Larose, L. Margerin, P. Roux, F. J. Sanchez-Sesma, N. M. Shapiro and R. L. Weaver, Cross-correlation of random fields: Mathematical approach and applications, *Geophysical Prospecting*, **56** (2008), 375–393.
[18] P. A. Martin, Acoustic scattering by inhomogeneous obstacles, *SIAM J. Appl. Math.,* **64** (2003), 297–308.
[19] P. M. Morse and K. U. Ingard, *Theoretical Acoustics*, McGraw-Hill, New York, 1968.
[20] G. Papanicolaou, L. Ryzhik and K. Sølna, Self-averaging from lateral diversity in the Ito-Schroedinger equation, *SIAM Journal on Multiscale Modeling and Simulation,* **6** (2007), 468–492.
[21] P. Roux, K. G. Sabra, W. A. Kuperman and A. Roux Ambient noise cross correlation in free space: Theoretical approach, *J. Acoust. Soc. Am.*, **117** (2005), 79–84.
[22] L. V. Ryzhik, G. C. Papanicolaou and J. B. Keller, Transport equations for elastic and other waves in random media, *Wave Motion*, **24** (1996), 327–370.
[23] N. M. Shapiro, M. Campillo, L. Stehly and M. H. Ritzwoller, High-resolution surface wave tomography from ambient noise, *Science*, **307** (2005), 1615–1618.
[24] P. Sheng, *Introduction to Wave Scattering, Localization, and Mesoscopic Phenomena*, Academic Press, San Diego, 1995.
[25] R. Snieder, Extracting the Green's function from the correlation of coda waves: A derivation based on stationary phase, *Phys. Rev. E*, **69** (2004), 046610.
[26] L. Stehly, M. Campillo, B. Froment and R. Weaver, Reconstructing Green's function by correlation of the coda of the correlation (C3) of ambient seismic noise, *J. Geophys. Res.,* **113** (2008), B11306.
[27] L. Stehly, M. Campillo and N. M. Shapiro, A study of the seismic noise from its long-range correlation properties, *Geophys. Res. Lett.*, **111** (2006), B10306.
[28] M. C. W. van Rossum and Th. M. Nieuwenhuizen, Multiple scattering of classical waves: Microscopy, mesoscopy, and diffusion, *Reviews of Modern Physics,* **71** (1999), 313–371.
[29] K. Wapenaar and J. Fokkema, Green's function representations for seismic interferometry, *Geophysics*, **71** (2006), SI33–SI46.
[30] R. Weaver and O. I. Lobkis, Ultrasonics without a source: Thermal fluctuation correlations at MHz frequencies, *Phys. Rev. Lett.*, **87** (2001), 134301.
[31] H. Yao, R. D. van der Hilst and M. V. de Hoop, Surface-wave array tomography in SE Tibet from ambient seismic noise and two-station analysis I. Phase velocity maps, *Geophysical Journal International*, **166** (2006), 732–744.

Received February 2012; revised June 2013.

E-mail address: garnier@math.univ-paris-diderot.fr
E-mail address: papanicolaou@stanford.edu